Geophysical Journal International

Geophys. J. Int. (2011) **184,** 268–286 doi: 10.1111/j.1365-246X.2010.04831.x

Upper-mantle seismic structure beneath SE and Central Brazil from *P*- and *S*-wave regional traveltime tomography

Marcelo Peres Rocha,[1] Martin Schimmel[2] and Marcelo Assumpção[3]

[1] *Institute of Geosciences, University of Brasília, Brasília, DF, Brazil. E-mail: peres_marcelo@yahoo.com.br*
[2] *Institute of Earth Sciences Jaume Almera – CSIC, Barcelona, Spain*
[3] *Department of Geophysics, IAG, University of São Paulo, São Paulo, SP, Brazil*

Accepted 2010 September 29. Received 2010 September 21; in original form 2009 May 7

SUMMARY

We present models for the upper-mantle velocity structure beneath SE and Central Brazil using independent tomographic inversions of *P*- and *S*-wave relative arrival-time residuals (including core phases) from teleseismic earthquakes. The events were recorded by a total of 92 stations deployed through different projects, institutions and time periods during the years 1992–2004. Our results show correlations with the main tectonic structures and reveal new anomalies not yet observed in previous works. All interpretations are based on robust anomalies, which appear in the different inversions for *P*- and *S*-waves. The resolution is variable through our study volume and has been analyzed through different theoretical test inversions. High-velocity anomalies are observed in the western portion of the São Francisco Craton, supporting the hypothesis that this Craton was part of a major Neoproterozoic plate (San Franciscan Plate). Low-velocity anomalies beneath the Tocantins Province (mainly fold belts between the Amazon and São Francisco Cratons) are interpreted as due to lithospheric thinning, which is consistent with the good correlation between intraplate seismicity and low-velocity anomalies in this region. Our results show that the basement of the Paraná Basin is formed by several blocks, separated by suture zones, according to model of Milani & Ramos. The slab of the Nazca Plate can be observed as a high-velocity anomaly beneath the Paraná Basin, between the depths of 700 and 1200 km. Further, we confirm the low-velocity anomaly in the NE area of the Paraná Basin which has been interpreted by VanDecar *et al.* as a fossil conduct of the Tristan da Cunha Plume related to the Paraná flood basalt eruptions during the opening of the South Atlantic.

Key words: Inverse theory; Mantle processes; Body waves; Seismic tomography; Dynamics of lithosphere and mantle; South America.

1 INTRODUCTION

1.1 Motivation

The South American continent is tectonically formed by the Andean orogeny in the west, the Precambrian South American Platform in the centre and east and the Late Paleozoic Patagonian Platform in the south (Ramos 1999; Almeida *et al.* 2000). The South American Platform occupies most of South America and is defined as the stable continental portion of the South American Plate, which has not been affected by the Phanerozoic (Andean and Caribbean) orogenic zones. The basement of the platform consists basically of Archean and Proterozoic lithospheric fragments (cratonic blocks) formed during the main Proterozoic orogenic events (Trans-Amazonian and Late Mesoproterozoic), which were finally linked by several Neoproterozoic mobile belts (Brasiliano/Pan African; Almeida *et al.* 2000). A schematic map of the main geological units is shown in Fig. 1.

Regional traveltime tomography is a powerful tool to obtain information about the upper mantle and uppermost lower mantle of the Earth. In Brazil, several tectonic domains have been imaged in previous tomographic studies (VanDecar *et al.* 1995; Schimmel *et al.* 2003; Assumpção *et al.* 2004a,b; Feng *et al.* 2004; Feng *et al.* 2007). However, due to the sparse and irregular distribution of earthquakes and seismic stations, the resolution is highly variable and some of the heterogeneities have been poorly resolved. In the mean time, the area covered by new stations has been increased and some stations have also been deployed in some of the poorly resolved areas. The main goal of this work is to study the main tectonic structures of the upper mantle under SE and Central Brazil (Fig. 1) using regional traveltime tomography for *P*- and *S*-waves. Main emphasis is given to the large-scale structures like the Tocantins Province, the São Francisco Craton (SFC), the Nazca Plate and the Paranapanema Cratonic Block. In this work, we want to shed light on some questions that still remain about the tectonic structure of the South America, such as the western limit of the SFC,

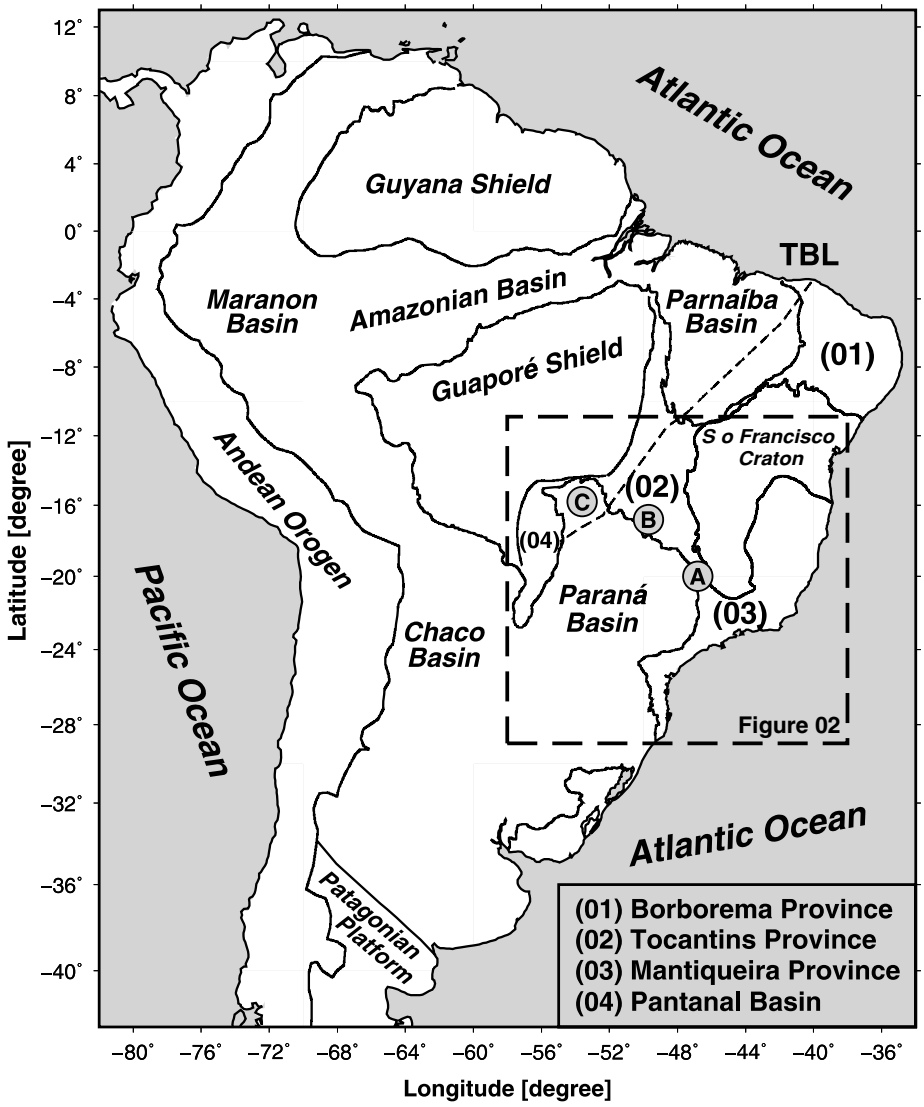

Figure 1. Tectonic map of the South America. Dashed square shows our study area. TBL stands for Trans-Brasiliano Lineament (thinner dashed line). 'A', 'B' and 'C' are the Alto do Paranaíba Igneous Province (APIP), the Iporá Igneous Province (IP) and the Poxoréu Igneous Province.

the layout of the cratonic basement of the Parana Basin, among others.

1.2 Tectonic settings

Our study area (thick dashed square in Figs 1 and 2) is completely contained in the South American Platform and comprises the following structural provinces: The SFC, the Tocantins and the Mantiqueira Provinces (mainly Brasiliano fold belts) and the Intracratonic Paraná Basin. Part of the uaporé Shield is included in the study area (Figs 1 and 2) but has not been sampled by our data.

The SFC is the best-exposed unit of the Precambrian Brazilian Shield (Teixeira *et al.* 2000). It is composed of an Archean and Paleoproterozoic crust and surrounded by Neoproterozoic Brasiliano/Pan African orogenic belts: Brasilia, Ribeira and Araçuaí (Alkmin & Cruz 2005).

The Tocantins Tectonic Province represents a large Brasiliano/Pan African orogen formed between three major continental blocks: the Amazonian, the São Francisco/Congo and the Paraná Cratons. This province contains three important supracrustal fold belts known as the Araguaia, the Paraguay and the Brasília Belts. The Araguaia and Paraguay Belts occupy the western part of this province, bordering the eastern and southern margins of the Amazonian Craton, respectively. The Brasília Belt forms the eastern part of the Tocantins Province, flanking the western edge of the SFC (Pimentel *et al.* 2000). The collision process that formed the Tocantins Province occurred in the Neoproterozoic, when the entire province was affected by the Brasiliano Orogenic Cycle. The main mega suture related to this event is the TransBrasiliano Lineament—TBL (thin dashed-line in Fig. 1) that crosses the entire region (Cordani *et al.* 2000). The TBL defines the boundaries of several different crustal domains to the NW, including the Amazonian Craton and to the SE, including mainly the SFC (Cordani & Sato 1999).

The Mantiqueira Province is an orogenic system comprising the Araçuaí, the Ribeira and the southern Brasília Fold Belts (among others), developed during the Neoproterozoic Brasiliano/Pan African Orogeny that resulted in the amalgamation of the Western Gondwana Paleocontinent (Heilbron *et al.* 2004; Silva *et al.* 2005).

The Paraná Basin, one of the three major intracratonic basins in eastern South America (e.g. Zalán *et al.* 1990; Milani &

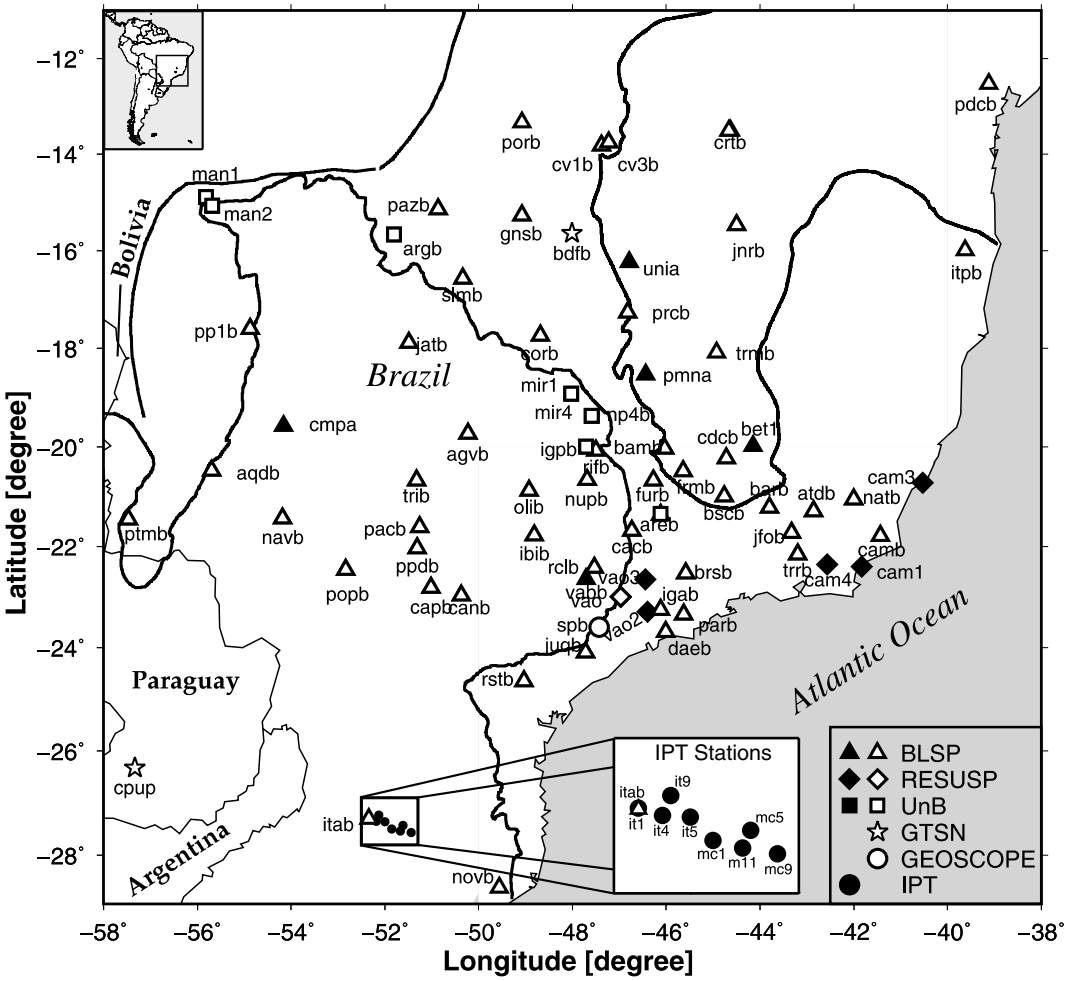

Figure 2. Study area with the stations used in this work. Different symbols represent stations of different projects or institutions. Black symbols are station used only for *P*-wave measurements (short period stations) and white symbols are stations used for both *P*- and *S*-wave measurements (broad-band stations).

Ramos 1998), is surrounded by late Proterozoic and Paleozoic Fold Belts (Brasília, Paraguay–Araguaia Belt and Ribeira) of the Brasiliano/Pan-African orogen (Almeida *et al.* 2000). On the basis of radiometric dates from two basement samples, a Proterozoic 'cratonic' nucleus was inferred beneath the Paraná Basin (Fyfe & Leonardos 1974; Cordani *et al.* 1984; Brito Neves & Cordani 1991). Cordani *et al.* (1984) named this unit as the Paraná Block.

Our study area includes several igneous provinces of alkaline intrusions with Late Cretaceous ages. The Late Cretaceous is recognized as the most important period for emplacement of alkaline complexes in South America (Montes-Lauar *et al.* 1995). The alkaline rocks are distributed around the Paraná Basin and comprise the Poxoréu, the Iporá, the Alto Paranaíba, the Serra do Mar and the Ponta Grossa Igneous Provinces (Gibson *et al.* 1995, 1997, 2005; Thompson *et al.* 1998; Siebel *et al.* 2000). Basically two age groups are found in our study area. The youngest group (85-60 Myr) tends to be located closer to the Atlantic Ocean and its spatial distribution suggests hotspot tracks. These younger igneous provinces may be related to a proposed Trindade Plume (Gibson *et al.* 1995, 1997). The oldest group (140-120 Myr) is located in the continental interior and is probably related to the impact of the Tristan da Cunha Super Plume during the South Atlantic rifting (e.g. Assumpção *et al.* 2004b).

1.3 Previous studies

The SFC has been observed as a high-velocity anomaly (mainly its southern part) in previous body-wave and surface-wave tomographies. Regional *P*- and *S*-wave traveltime tomography (VanDecar *et al.* 1995; Schimmel *et al.* 2003) showed that the roots of this craton are about 200 and 250 km deep whereas results of surface-wave tomography (Feng *et al.* 2004; Heintz *et al.* 2005; Feng *et al.* 2007) indicate depths down to 150–200 km. The western limit of the SFC has been a controversial matter (Alkmin *et al.* 1993; Ussami 1993). Several seismic studies compiled by Assumpção *et al.* (2004a) indicate that the western limit of the SFC extends further to the west, beneath the foreland domain of the Brasilia Fold Belt (Alkmin *et al*. 1993). Assumpção *et al.* (2006) compared the results of SK(K)S splitting observations with the *S*-wave anomalies in Central and SE Brazil and observed a clear fan shaped pattern around the keel of the SFC. These observations suggest that the asthenospheric flow is locally deflected by the lithosphere/asthenosphere topography beneath this Craton and support the hypothesis that the SFC is part of a major Neoproterozoic plate (San Franciscan Plate).

Schimmel *et al.* (2003) also observed high-velocity anomalies of *P*- and *S*-waves in the upper mantle beneath the central and western Paraná Basin, which would be consistent with the presence of a cratonic nucleus buried under the sediments and flood basalts of the

Paraná Basin. The nature of the basement beneath the Paraná Basin is still debated. The single cratonic nucleus proposed initially by Cordani *et al.* (1984) and Zalán *et al.* (1990) has been contested by Milani & Ramos (1998) who propose several smaller blocks separated by mobile belts, rifting and alkaline magmatism. Recently, a third model (Mantovani *et al.* 2005) of a larger 'Paranapanema block' has been suggested based mainly on gravity anomalies. Previous tomographic results (both, body and surface-wave) did not have enough resolution to distinguish between the proposed models due to a small amount of stations in this area. Julià *et al.* (2008) analysed the crustal structure beneath several stations in the Paraná Basin and favoured the model of Milani & Ramos (1998).

VanDecar *et al.* (1995) detected a low-velocity cylindrical structure in the upper mantle beneath the NE part of the Paraná Basin. With the increase of the number of stations, Schimmel *et al.* (2003) found that this anomaly is confined to the whole upper mantle, although it appears as a continuous feature down to about 900 km. Schimmel *et al.* (2003) interpreted this downwards extension as an artefact due to vertical smearing caused by fewer ray crossings at the top of the lower mantle. This low-velocity anomaly was observed down to 300 km depth by Feng *et al.* (2007) using surface wave tomography, (greater depths are not resolved by their study). The causes of this seismic anomaly remain uncertain, however. VanDecar *et al.* (1995) interpreted this structure as a fossil conduit through which the initial Tristan da Cunha Plume travelled to generate the Paraná–Etendeka continental flood basalts. Imaging of the 410 and 660 km seismic velocity discontinuities, along an E–W profile across South America ($\sim$20°S; Liu *et al.* 2003), indicates a slight thickening of the transition zone rather than the expected thinning for a hot thermal anomaly in an olivine dominated transition zone, thus indicating a chemical anomaly. Van der Lee & Wiens (2006) suggest a compositional explanation for this anomaly related to the water release from the deep subducted Nazca slab.

At depths of 150–250 km, low-velocity anomalies predominate in the fold belt areas, which are mostly correlated with the Late Cretaceous Igneous Provinces (VanDecar *et al.* 1995; Schimmel *et al.* 2003; Assumpção *et al.* 2004a). Schimmel *et al.* (2003) and Assumpção *et al.* (2004a) observed a low-velocity anomaly near the Alto do Paranaíba Igneous Province–APIP (A in Fig. 1). The fact that only the more recent (85–50 Ma) alkaline intrusions occur near low-velocity areas may indicate a thermal effect associated with the generation of the Late Cretaceous igneous activity. A *P*-wave low-velocity anomaly was also observed under the Iporá Igneous Province–IP (B in Fig. 1; Assumpção *et al.* 2004a) and was interpreted as the initial impact of the Trindade Plume at $\sim$80 Ma, as proposed by Gibson *et al.* (1997). Rocha (2003) and Assumpção *et al.* (2004a) also observed a low-velocity trend beneath the Poxoréu Igneous Province–PX (C in Fig. 1) and suggested that this anomaly could be part of the Trindade Plume impact. Both anomalies could be related to the TBL, indicating a thin and weak lithosphere in this region (Assumpção *et al.* 2004a). Feng *et al.* (2004, 2007) also found in this region a NE–SW trending low-velocity anomaly at about 100 km depth, possibly related with the TBL. Low-velocity anomalies were also observed in the Serra do Mar and Ponta Grossa Provinces (Escalante 2002; Rocha 2003; Schimmel *et al.* 2003).

Assumpção *et al.* (2004a) show a positive correlation between *P*-wave low-velocity anomalies and the areas with greater seismicity in SE and Central Brazil. They suggested that the lithosphere/asthenosphere topography, inferred from *P*-wave tomography, is in excellent agreement with the thin spot hypothesis proposed by Gibson *et al.* (1995, 1997) for the origin of the igneous provinces and still, that the thinning of the lithosphere induced by temperature can be an important mechanism to help explain earthquake activity in SE and Central Brazil.

A study of the effective elastic thickness of the lithosphere (*Te*) in South America (Pérez-Gussinyé *et al.* 2007) shows low *Te* in the Pantanal Basin and the SE part of the TBL, coincident with low-velocity anomalies and consistent with a thin and weak lithosphere in these areas. Greater *Te* was observed, mainly, in cratonic regions.

Schimmel *et al.* (2003) found an N–S oriented high-velocity anomaly in the upper mantle, which they interpreted as due to the subducted Nazca Plate. Their synthetic tests show that a continuous slab is imaged as two separated slab segments, suggesting low resolution in the lower mantle. Ren *et al.* (2007) combine tomography with plate tectonic history to track the subduction underneath the Americas in time. Also in their images the Nazca/Farallon slab is less well resolved beneath SW Brazil. Both studies do not show a continuation of this segment below about 1300 km depth.

2 DATA

2.1 Station and event selection

We used relative traveltime residuals obtained from teleseismic events. These data were recorded by a total of 92 stations deployed for different durations in the study area (Fig. 2), during 12 yr (1992–2004). Relative residuals were obtained from waveform cross-correlations for up to 12 simultaneously recorded seismograms. We included 5647 *P*-wave and 3466 *S*-waves traveltime measurements from new stations (2000–2004) in the previous database of Schimmel *et al.* (2003), who used events from 1992 to 2000.

Most of the stations were from the BLSP (Brazilian Lithosphere Seismic Project—BLSP92, BLSP95 and BLSP02) equipped with three-component broad-band seismometers. Stations from others projects and institutions were also used: RESUSP—University of São Paulo Seismic Network; UnB-–University of Brasília; IPT—Institute of Technological Research; GTSN—Global Telemetered Seismic Network; GEOSCOPE Institut de Physique du Globe de Paris. Only data from broad-band stations were employed in our *S*-wave study, while we have used also short-period stations to increase the database for the *P*-waves. The waveforms of the short period instruments have been transformed to mimic broad-band records and have been used together with the vertical broad-band data at narrow frequency bands around 1 Hz.

P- and *S*-phases were used from events with magnitude larger than 4.6 mb. For direct (*P* and *S*) and core reflected phases (ScS), the epicentral distances range from 30° to 95° and 10° to 30°, respectively. Further, we used core-refracted phases (PKPdf, SKS, SKKS) from events at 100° to 180°. The USGS PDE (U.S. Geological Survey Preliminary Determination of Epicenters) database provided the hypocentre information. Fig. 3 shows the distribution of these earthquakes.

2.2 The relative arrival-time determination

We use relative traveltime residuals to decrease source errors and path effects outside the investigated volume (Evans & Achauer 1993). The relative traveltime residuals have been determined using

$$r_{ij} = to_{ij} - tc_{ij} \quad \Rightarrow \quad rr_{ij} = r_{ij} - \frac{1}{N}\sum_{i=1}^{N} r_{ij}, \tag{1}$$

where r_{ij} is the absolute residual for station i and event j. to and tc stand for observed and theoretical traveltime, respectively. rr_{ij} is the relative residual used to build our database.

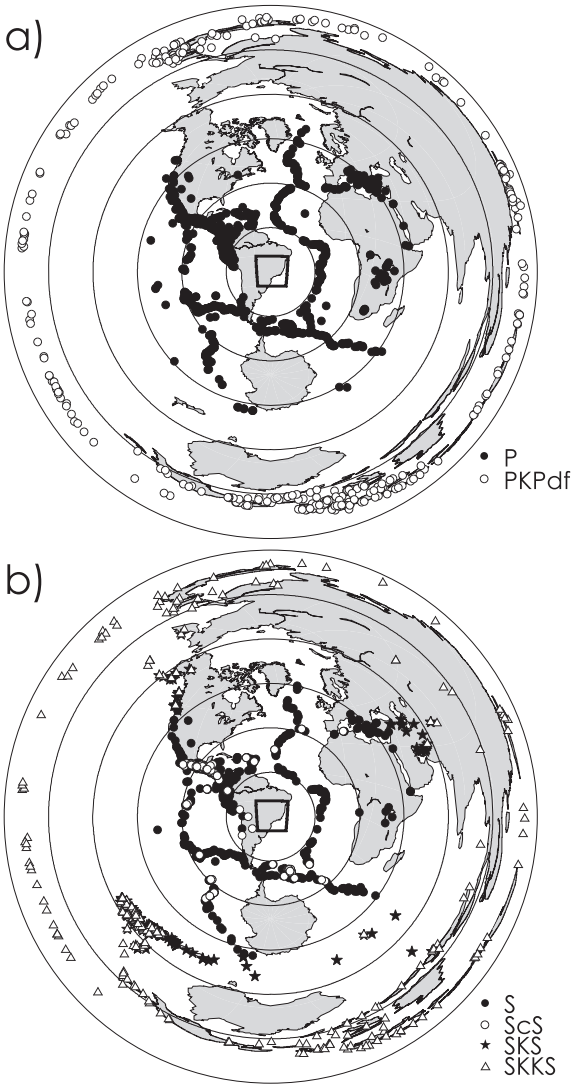

Figure 3. Distribution of the events used in this work. Distances are with respect to the centre of the study area (black square). (a) *P*-wave events. (b) *S*-wave events.

Relative traveltimes were measured using the MultiChannel Phase Cross Correlation (MCPCC) technique (Schimmel *et al.* 2003), which incorporates the Phase Cross-Correlation (PCC) function (Schimmel 1999) into the MultiChannel Cross Correlation technique of VanDecar & Crosson (1990). MCPCC uses the similarity of the greatest number of coherent samples rather than the largest sum of cross products. Therefore, it is not biased by the large amplitude portions in the correlation window. The data were inspected event by event and the correlation windows were selected by hand to include the first swing of the signal. The correlation results were manually checked to avoid cycle skipping or other problems. Poor signals were correlated using different parameters and discarded if not providing satisfactory and consistent results.

Picking of *P*- and *S*-wave phases was performed at a high-frequency band because our inversion procedure adopts ray theory (the infinite frequency approximation for wave propagation). The bandwidths for *P*- and *S*-waves range between 0.8–2.5 Hz and 0.05–0.1 Hz, respectively. The corresponding wavelengths in the upper-mantle are about 12 km for *P*-waves and 60 km for *S*-waves. The *S* and ScS phases were picked on the tangential components to minimize contamination by *P*- and *P*-to-*S* converted waves. Core phases (SKS and SKKS) were picked on the radial components where they are strongest due to their *P*-wave path in the outer core.

2.3 The final data sets

The final database consists of 8551 time measures for *P*-waves (1240 events), 2463 for PKP (338 events), 4707 for *S* (734 events), 697 for ScS (106 events), 1109 for SKSac (171 events) and 1719 for SKKSac (262 events). The traveltimes were corrected for station elevations using the theoretical ray incidence in an upper crust with *P*-wave velocity of 5.8 km s^{-1} and *S*-wave velocity of 3.5 km s^{-1}. Our *P*- and *S*-wave relative residuals follow a normal distribution (Fig. 4). The standard deviations for the *P*- and *S*-wave data are 0.407 s and 1.096 s, respectively. The comparison between the data distribution and the Gaussian curve allows to find large traveltime residuals, which have been removed since they are likely due to timing errors or phase misinterpretations and could influence the inversion.

3 METHOD

3.1 Model parameterization

The model has been discretized in a dense grid of knots, which is interpolated with splines under tension (Cline 1981, Neele *et al.* 1993) to obtain the seismic velocities at each location within the grid. This interpolation scheme provides a smooth slowness distribution and therefore permits an accurate ray tracing. The grid is composed of 64 260 knots, 28 knots in depth (depths between 0–1400 km), 45 knots in latitude (latitudes between –30° and –10°) and 51 knots in longitude (longitudes between –59° and –37°). In the central region of the model (25-15°S; 53-40°W; 0–500 km depth), where we expect to obtain better resolution, the horizontal and vertical knot spacing is 1/3 degrees and 33km, respectively. The knot spacing increases outside this region to 0.5° and 50 km in an intermediate volume and to 1° and 100 km outside this intermediate volume. The parameterization extends outside the area of the stations to minimize the mapping of noise and inconsistencies as unrealistic structures into the central area of interest (VanDecar *et al.* 1995).

Note that the hypocenters of all events are outside the study volume and there are no significant down going ScS ray path within the volume. In our inversion only upgoing ScS rays will be considered.

3.2 Inversion procedure

We use the linear inversion approach of VanDecar *et al.* (1995) which has been a successful tool to study the upper mantle in different areas (e.g. VanDecar *et al.* 1995; Sol *et al.* 2002; Wolfe *et al.* 2002; Schimmel *et al.* 2003; Bastow *et al.* 2005; Benoit *et al.* 2006; Lees *et al.* 2007; Bastow *et al.* 2008; Schmid *et al.* 2008; West *et al.* 2009). In this method, *P*- and *S*-wave relative residuals are independently inverted for 3-D velocity structure (velocity anomalies), earthquake relocations and station terms. The station terms are used in the inversion to absorb systematic time contributions caused by local shallow heterogeneities. Also, the source terms are used to account for small source mislocations.

The linear system of equations is underdetermined which means the inversion is non-unique and different solutions are possible to explain the data. For this reason we look for smooth models with

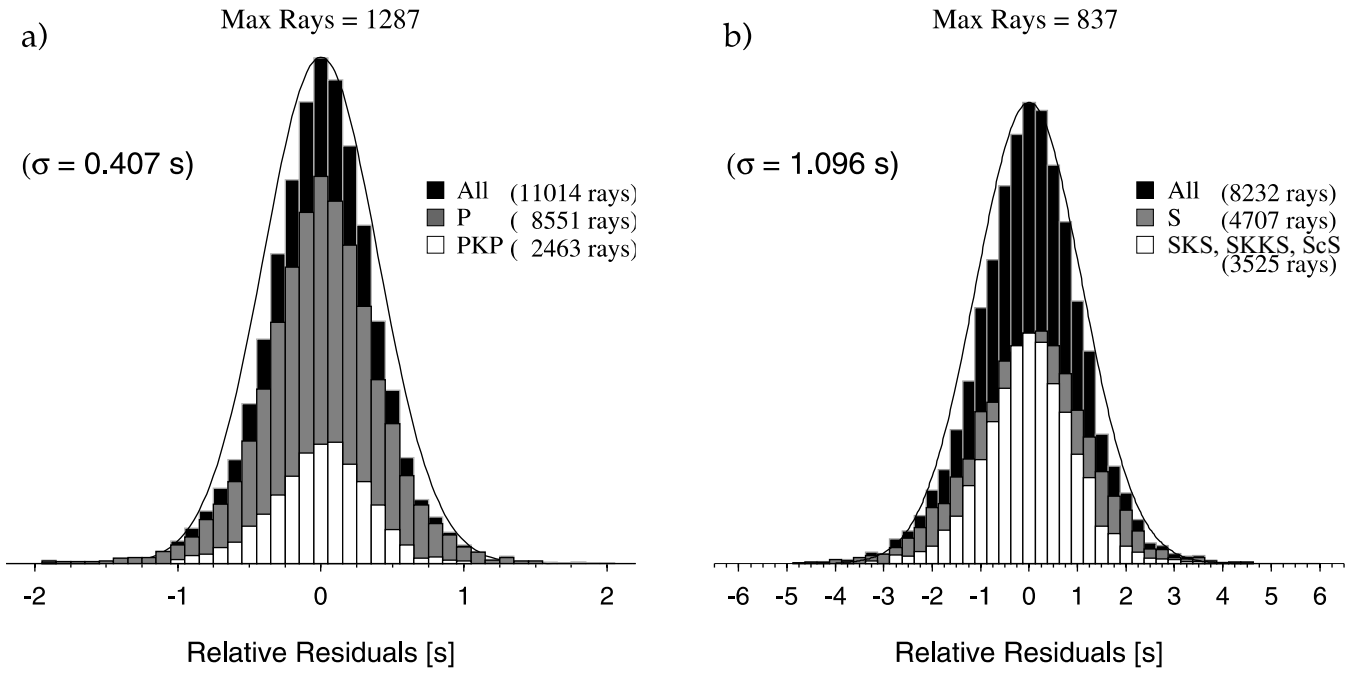

Figure 4. Histograms for the relative *P*-wave (a) and *S*-wave (b) residuals. Core phases and first arrival distributions are illustrated in white and grey, respectively and the distribution of all phases is shown in black.

the least amount of anomalies to explain the relative time residuals (Occam's inversion – Constable *et al.* 1987) by including regularization through a combination of the first- and second-order difference operators. The linear system is inverted iteratively using the conjugate gradient method LSQR (Paige & Saunders 1982a,b). We iterate upon these inversions, systematically down-weighting equations associated with outlying residuals from the previous iteration (Huber 1981). This approach produces a robust solution with L2 residual minimization for data with residuals smaller than 1.5 times the standard deviation and L1 residual minimization for equations associated with larger residuals (e.g. Pulliam *et al.* 1993).

The down-weighting iterations are interrupted when the anomalies do not show significant variations from the previous iteration. Our final models explain about 84 per cent of the rms relative residual of the original data set (from 0.41 to 0.06 s) for *P*-waves and about 86 per cent of the rms residual (from 1.10 to 0.15 s) for *S*-waves. We subtracted the station static terms from the delay times to estimate the proportion of the residuals that are absorbed by the static terms. The rms of the relative residual was reduced from 0.40 to 0.39 s for *P*-waves and from 1.10 to 1.07 for *S*-waves. This indicates that about 3 per cent of the rms of the relative residuals is absorbed by the station terms and about 81 per cent of the residuals are inverted into structure (*P*-waves), since the total rms reduction is in the order of 84 per cent.

4 UPPER-MANTLE SEISMIC STRUCTURE

Our results are presented as horizontal (Figs 5 and 6) and vertical sections (Fig. 7). These Figures show velocity perturbations relative to the IASP91 Earth model (Kennett & Engdahl 1991). Areas with ray density less than 20 rays 100 km^{-3} are shown in black. In the vertical cross-sections the first 50 km are blacked since there is no ray crossing immediately underneath the stations, which means that there is no resolution. White squares are stations and yellow circles (only in Figs 5a and 6a) are the Late Cretaceous alkaline intrusions (90-55 Ma). The final *P*- and *S*- velocity anomaly models contain similar features although they were obtained independently. The *S*-wave anomalies are more blurred than the *P*-wave anomalies. This effect is explained by the lower resolution of the *S*-waves compared with *P*-waves, based on their larger Fresnel volumes.

4.1 São Francisco Craton

After the installation of new stations in the northern part of the SFC, high-velocities at lithospheric depths are observed in this region (Figs 5a and b; 6a and b). However, the anomaly in the southern part is more intense than in the northern part, due to its better resolution as shown later. A high-velocity anomaly west of the surface limit of the SFC supports the hypothesis that this craton was part of a major Neoproterozoic plate (San Franciscan Plate—Alkmin *et al.* 1993; Ussami 1993, 1999). In the vertical cross-sections (Figs 7a and b), the SFC appears as a high-velocity anomaly down to about 300 km depth. However, the craton is less deep due to smearing along the dominantly steep ray paths as shown in our resolution tests.

4.2 Basement of the Paraná Basin

The high-velocity anomaly observed by Schimmel *et al.* (2003), beneath the Paraná Basin and interpreted as a cratonic block, is confirmed in our results (Figs 5a and b; 6a and b and 7c and d). This anomaly appears with an improved horizontal resolution (based on synthetic tests). However, despite the increased database, its vertical resolution remained poor, due to few ray crossings and an excess of ray paths from the Andes. This prevents a clear separation of the possible high-velocity lithosphere beneath the Paraná Basin from

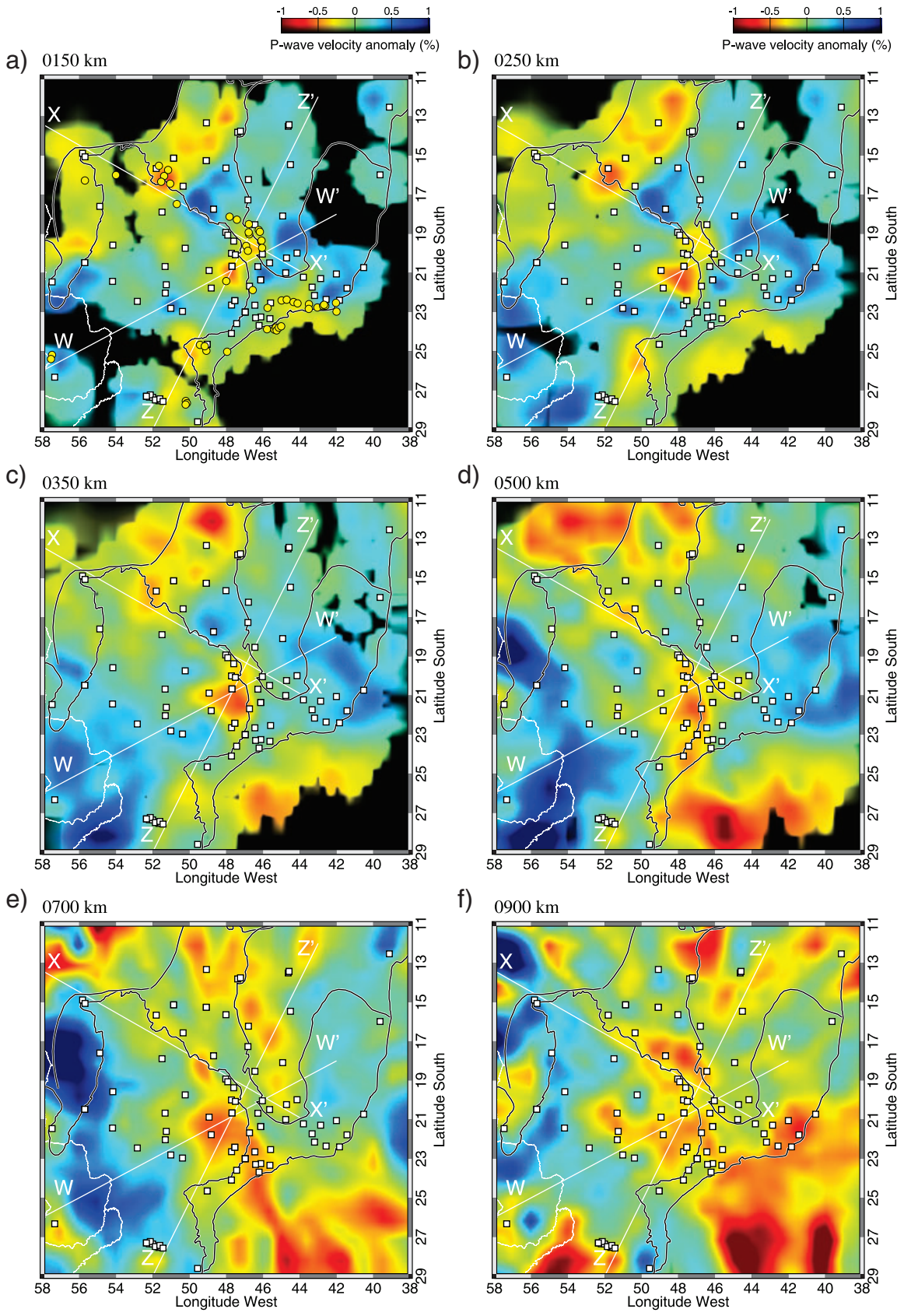

Figure 5. Horizontal tomographic images for the depths of 150, 250, 350, 500, 700 and 900 km for *P*-wave velocity anomalies. The thick lines indicate the main geologic structures and the white lines mark the vertical profiles (Fig. 7). The white squares and yellow circles mark the stations and the alkaline intrusions of the Upper Cretaceous, respectively.

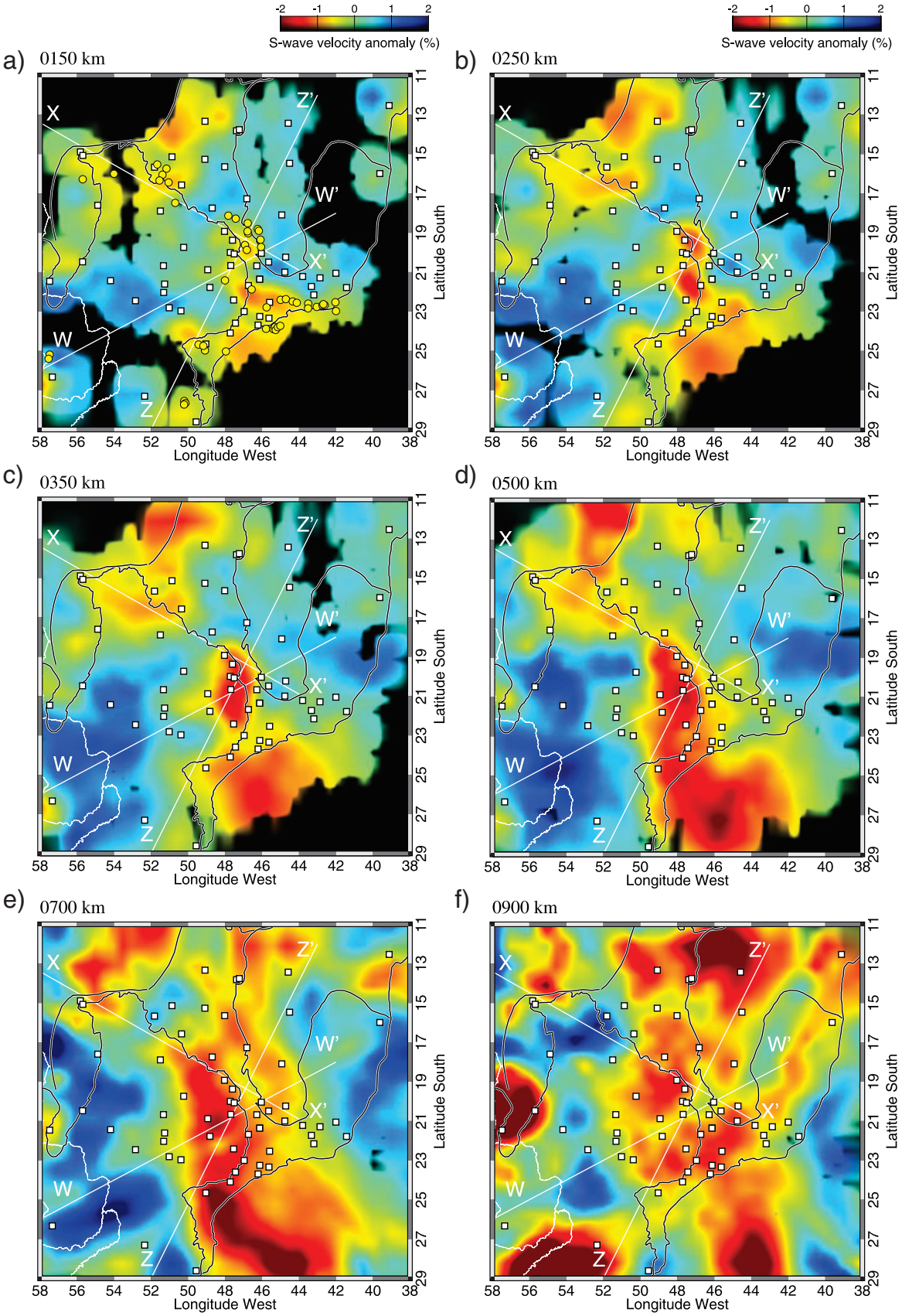

Figure 6. Horizontal tomographic images for the depths of 150, 250, 350, 500, 700 and 900 km for *S*-wave velocity anomalies. The thick lines indicate the main geologic structures and the white lines the vertical profiles (Fig. 7). The white squares and yellow circles mark the stations and the alkaline intrusions of the Upper Cretaceous, respectively.

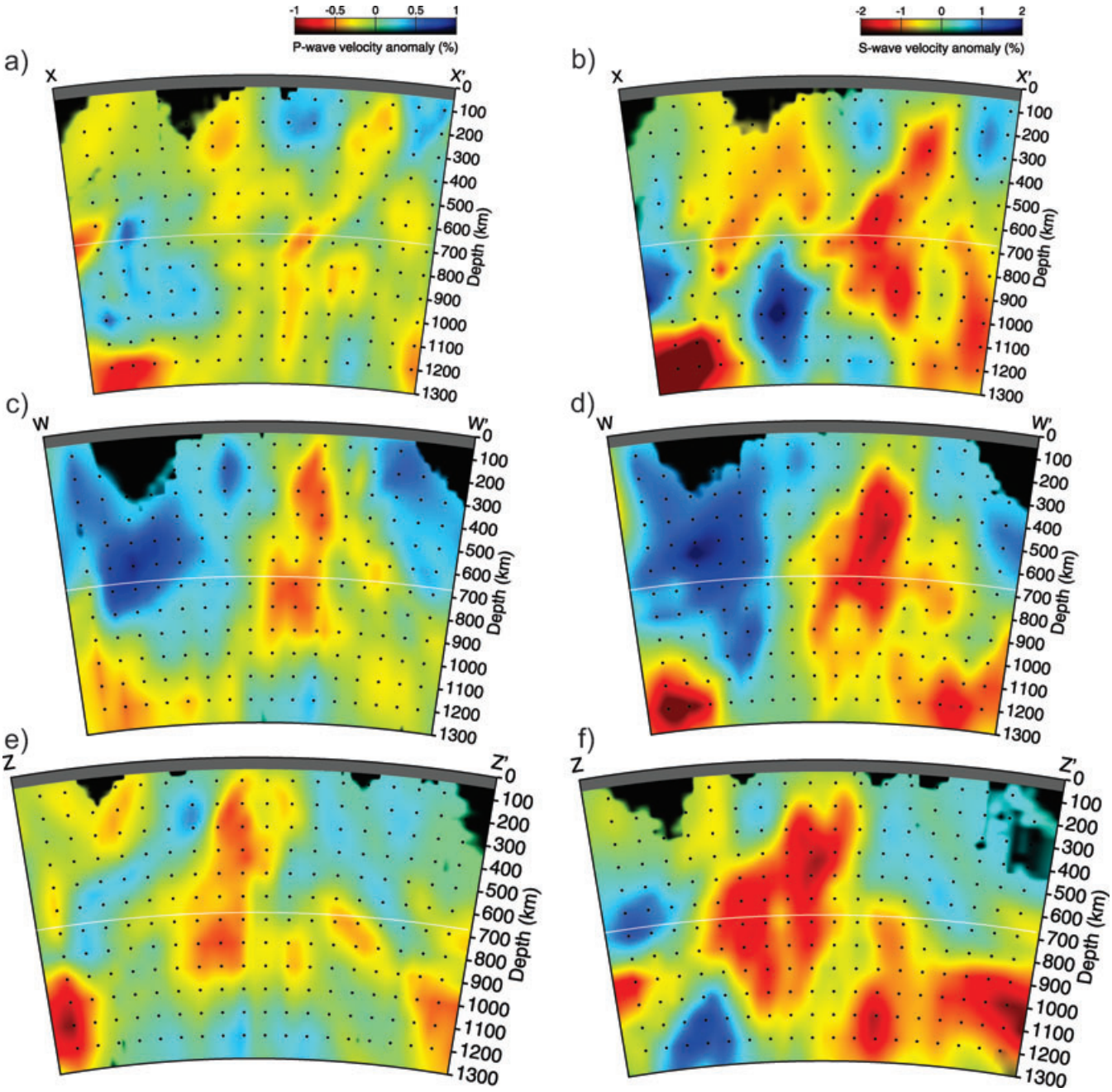

Figure 7. Vertical cross-sections for *P*- (a, c and e) and *S*-wave (b, d and f) velocity anomalies. See Figs 5 and 6 for their positions.

a deeper anomaly related to the subducted Nazca slab (Figs 7c and d).

4.3 NE Paraná 'Fossil Plume'

The low-velocity anomaly observed by VanDecar *et al.* (1995), located in the northeast limit of the Paraná Basin, is also observed in our results (Figs 5c–f; 6c–f and 7). VanDecar *et al.* (1995) interpreted this anomaly as the fossil conduct of the initial Tristan da Cunha Plume. This anomaly reaches depths down to 900 km. Another large low-velocity anomaly is observed together (mainly for *S*-waves) at depths larger than 700 km (Fig. 7). We believe that this other low-velocity is an artefact generated by the inversion as shown in the synthetic tests.

4.4 Low-velocity anomalies and Cretaceous Igneous Provinces

A low-velocity anomaly in the region of the Iporá Igneous Province, at a depth of about 200 km, is observed in our *P*- and *S*-wave results (Figs 5a–c; 6a–c and 7a and b). A second low-velocity anomaly was observed in the region of the Poxoréu Igneous Province (Figs 5a–c; 6a–c and 7a and b). These two anomalies could be related with the initial impact of the Trindade Plume (Thompson *et al.* 1998), or with the TBL (Cordani & Sato 1999).

We also observe a low-velocity anomaly geographically correlated with the APIP (Figs 5c–f; 6c–f and 7), and in the region of the Serra do Mar Igneous Province and the Ponta Grossa Arc (Figs 5a and b; 6a and b and 7e and f).

4.5 Nazca slab

The deep high-velocity anomaly beneath the Paraná Basin interpreted by Schimmel *et al.* (2003) as the slab of the Nazca Plate is also observed in our results. It has a NW–SE orientation (Figs 5c–e and 6c–e), according with the Nazca contour between the latitudes –16° and –30°. Schimmel *et al.* (2003) observed the slab segmented into two parts, but they show that they do not have the resolution to distinguish between a continuous or segmented slab. A possible fragmentation still cannot be resolved due to the smearing of the seismic anomalies.

5 RESOLUTION

The resolution of the tomographic images depends on several factors, such as the spatial distribution of data, parameterization of the study region, among others. Synthetic tests with known seismic structures are normally used to assess the resolution of the tomographic results (e.g. Schimmel *et al.* 2003; Bastow *et al.* 2005; Rawlinson *et al.* 2006).

We inverted synthetic traveltimes, calculated with a 3-D ray tracer for geometric input models by using the real event/station configuration. The geometric models are often used for resolution tests and are based on simulations of one or more tectonic features indicated by the real data or geological information (e.g. Schimmel *et al.* 2003; Bastow *et al.* 2005). A Gaussian residual time error component, with a standard deviation of 30 per cent of the rms of the synthetic data residuals, was added to the traveltimes to generate noisy data and to see how this data inconsistency affects the inversion results.

The different synthetic input models and the respective tomographic reconstructions are shown in the Fig. 8 (horizontal cross-sections) and Fig. 9 (vertical cross-sections). As high-velocity structures we have the SFC, Paranapanema Craton (PC) and Nazca Plate (NP) and as low-velocity anomalies we have the Iporá Igneous Province (IP), Poxoréu Igneous Province (PX), Alto do Paranaíba Igneous Province (AP), Ponta Grossa Arc (APG), Pantanal Basin (PT) and the anomaly interpreted by VanDecar *et al.* (1995) as Tristan da Cunha Plume head (TC). Model 1 uses all these structures and Model 2 consists only of high-velocity anomalies. Model 3 is similar to Model 1 except for the NP. The SFC extends down to 150 km, 200 km and 250 km depth for Model 1, Model 2 and Model 3, respectively, to estimate its depth resolution.

Comparisons between real (Figs 5a and 6a) and synthetic results (Fig. 8f) show a good correlation between the images in areas with good station coverage (central part of the model). The results of the resolution tests show that the lithospheric structures (Figs 8c and 9f) are best resolved for the data from Model 3 (without NP). It can be seen that the anomalies are smeared in depth, which is due to the dominantly steep ray paths. Owing to this effect, the presence of the slab in the Model 1 interferes with shallower structures and decreases their amplitudes. We believe that the slab orientation is not NS (as modelled) since, in the real results, the amplitudes of the northern anomalies do not decrease significantly, suggesting that its orientation is concordant with the outline of the convergence between the South American and Nazca Plates. In the vertical cross-sections (Fig. 9) we observed that NP and PC cannot be resolved due to the mentioned smearing along the large concentration of ray paths from the Andes.

Comparing the results of the synthetic tests of the three models (Fig. 9) with the real data inversions (Fig. 7) we observed that the south part of SFC should be deeper than 200 km. In the northern part however, due to the low resolution caused by the low station density, it is not possible to propose depth limits. The western extension, interpreted as the 'San Franciscan Plate', has good resolution, similar to the southern part of this craton.

A large low-velocity anomaly appears in the lower mantle next to the simulated NP (Figs 8 and 9). This anomaly is an artefact generated during the inversion, because there are no low-velocity anomalies at these depths in our model. Model 2 (Figs 8 and 9) contains no low-velocity anomalies at all and still, the lower mantle artefacts remain and are therefore not due to mis-mapping or smearing of other low-velocity bodies. Only the removal of the slab (Model 3, Figs 8 and 9) causes the disappearance of the artefacts in the reconstructions. We attribute this problem to the poor resolution in the lower mantle. A similar low-velocity anomaly appears in the real data inversions (Figs 5 and 6—depths 500–900) and can be used as further hint to the presence of the slab.

In general, we observe in the synthetic tests that the central part of the model has best resolution due to the highest density of crossing rays in this area. AP and TC have therefore good lateral and vertical resolution. The APG amplitude is slightly lower in the Model 1 (with NP) if compared with the Model 3 (without NP), probably due to the strong influence of the presence of NP that decreases the low velocity amplitudes.

The percentage velocity scale has been reduced to show the full range of amplitudes. The recovered synthetic models are smooth since strong spatial velocity gradients are reduced through the regularization of the inversion. The amplitudes of the anomalies are underestimated in the real data inversions since they represent the minimum structure required to explain the data.

6 CAUSES OF SEISMIC HETEROGENEITY

The origin of lateral seismic heterogeneities in the Earth's mantle is one of the most important issues in geodynamical applications of seismic tomography. In particular, distinguishing thermal from compositional origin of heterogeneities is important because the dynamic implication is quite different between the two cases (Karato & Karki 2001). In the upper mantle, temperature is believed to have more influence than compositional variations in the origin of the seismic heterogeneities (e.g. Goes *et al.* 2000). However, other studies showed that a significant part of the seismic anomalies in the upper mantle cannot be explained by thermal variations (e.g. Deschamps *et al.* 2002; Artemieva *et al.* 2004).

In this study, we cannot distinguish between the different origins of heterogeneities from our inversion since we do not resolve absolute velocities, since the ray path for *P*- and *S*-waves are different, and since the *P*- and *S*-wave inversions have different resolutions. Nevertheless, a comparison between *P*- and *S*-wave relative arrival-time residuals for common station and event pairs is sometimes used to compare directly the velocity anomalies of the tomographic images (Bastow *et al.* 2005). This procedure avoids all the problems associated with amplitude recovery (e.g. due to differing numbers of traveltime observations and regularization levels) and other artefacts associated with the inversion procedure, such as parameterization and ray path accuracy.

Fig. 10(a) shows *S*- versus *P*-wave relative traveltime residuals for common earthquake—station pairs. The *P*- and *S*-wave data are measured independently and sample slightly different structures, but are positively correlated as expected. The best fitting

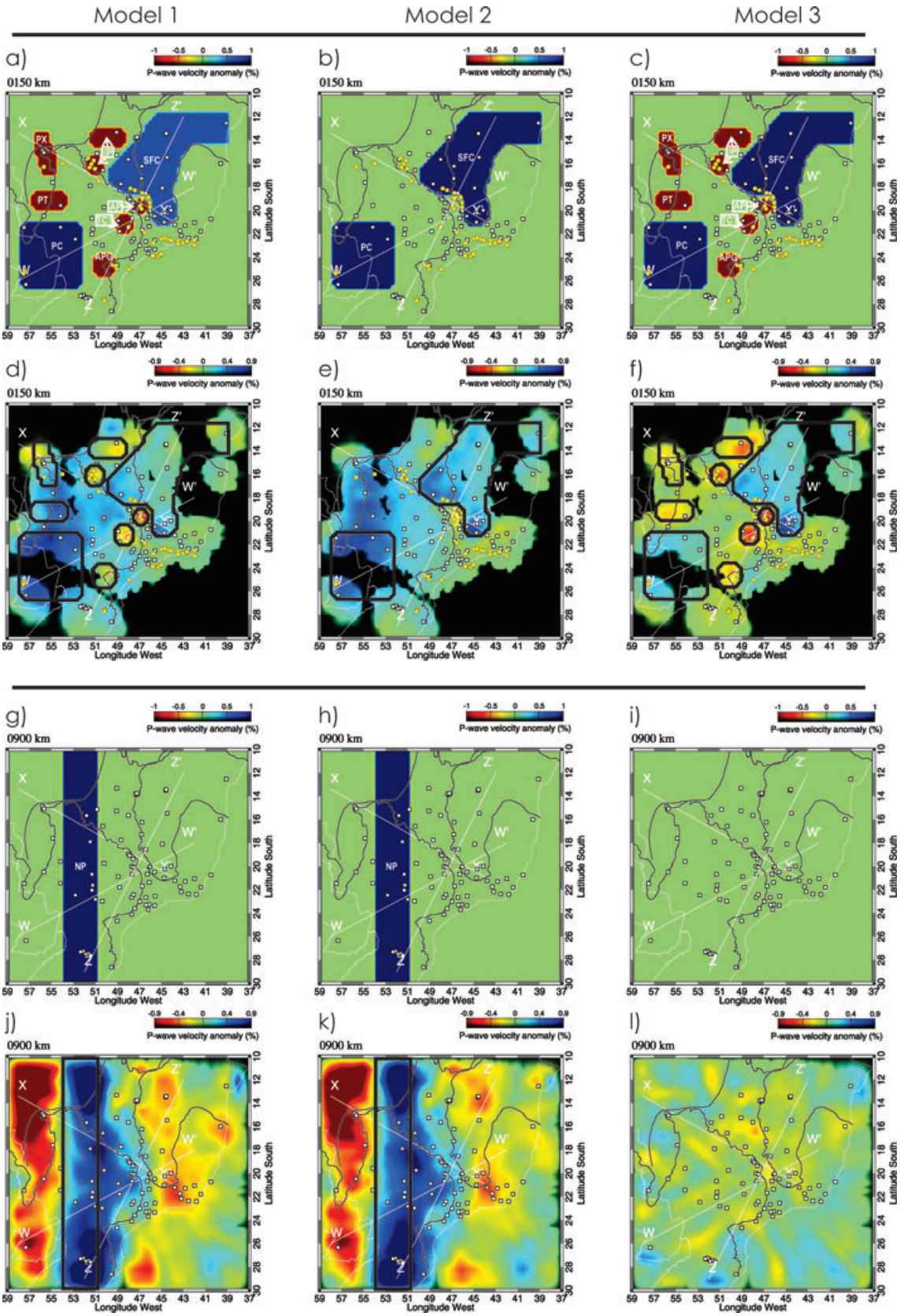

Figure 8. Geometric synthetic models to analyse the resolution of the main tectonic structures between 150 and 900 km depth. (a), (b), (c) and (g), (h), (i) are the input models and (d), (e), (f) and (j), (k), (l) are their reconstructions for 150 km and 900 km, respectively. Following abbreviations are used: SFC, São Francisco Craton; PC, Paranapanema Craton; NP, Nazca Plate; IP, Ipora Igneous Province; AP, Alto do Paranaíba Igneous Province; PT, Pantanal Basin and TC, fossil conduct of the Tristan da Cunha Plume (VanDecar *et al.* 1995).

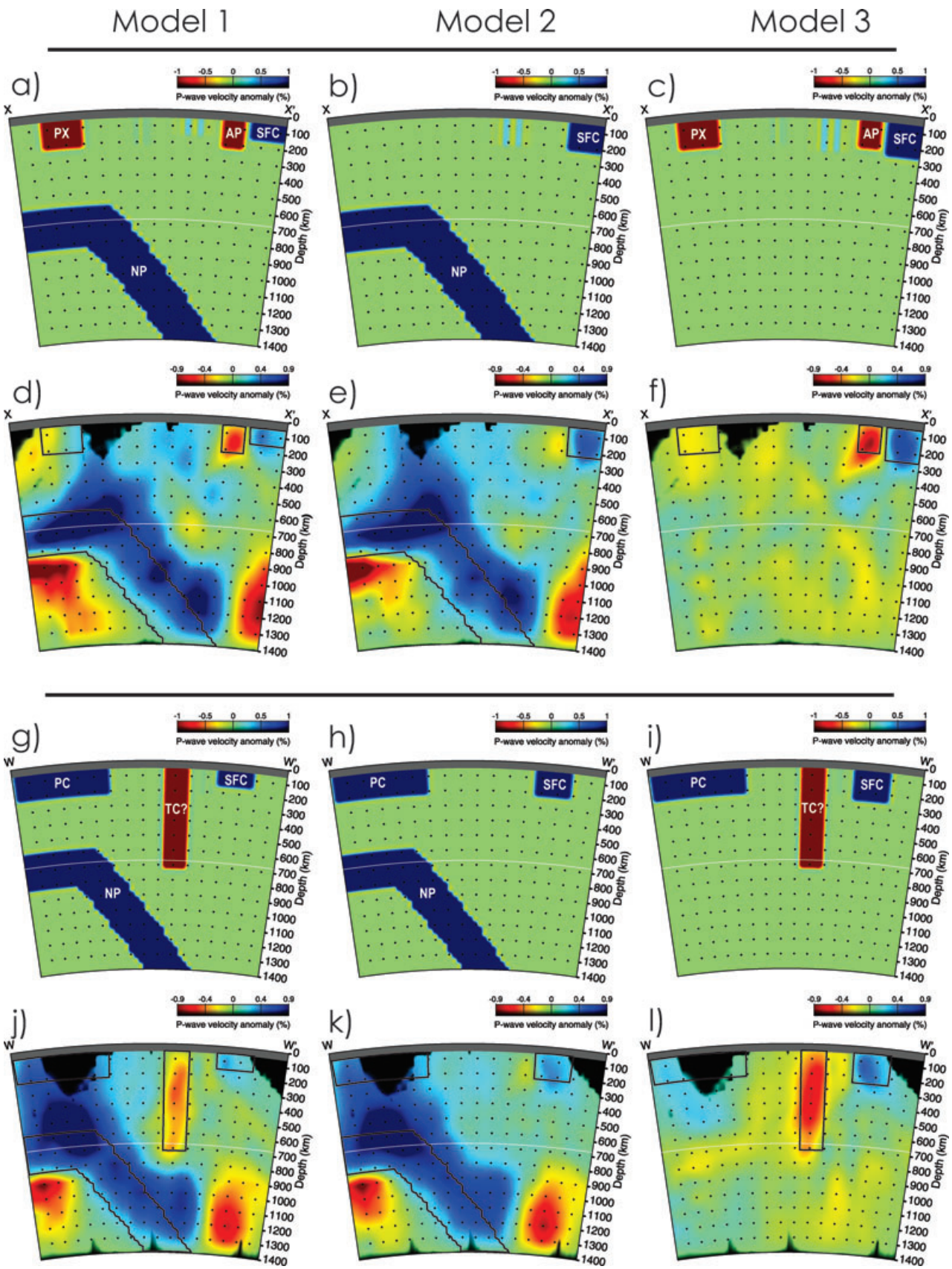

Figure 9. Geometric synthetic models (vertical profiles) to analyse the resolution of the main tectonic structures in our study area. (a), (b) and (c) are the input models for profile X–X′ and (d), (e) and (f) are the results of the inversions for this profile. (g), (h) and (i) are the input models profile W–W′ and (j), (k) and (l) are the results of the inversions for this profile. See Fig. 8 for abbreviations.

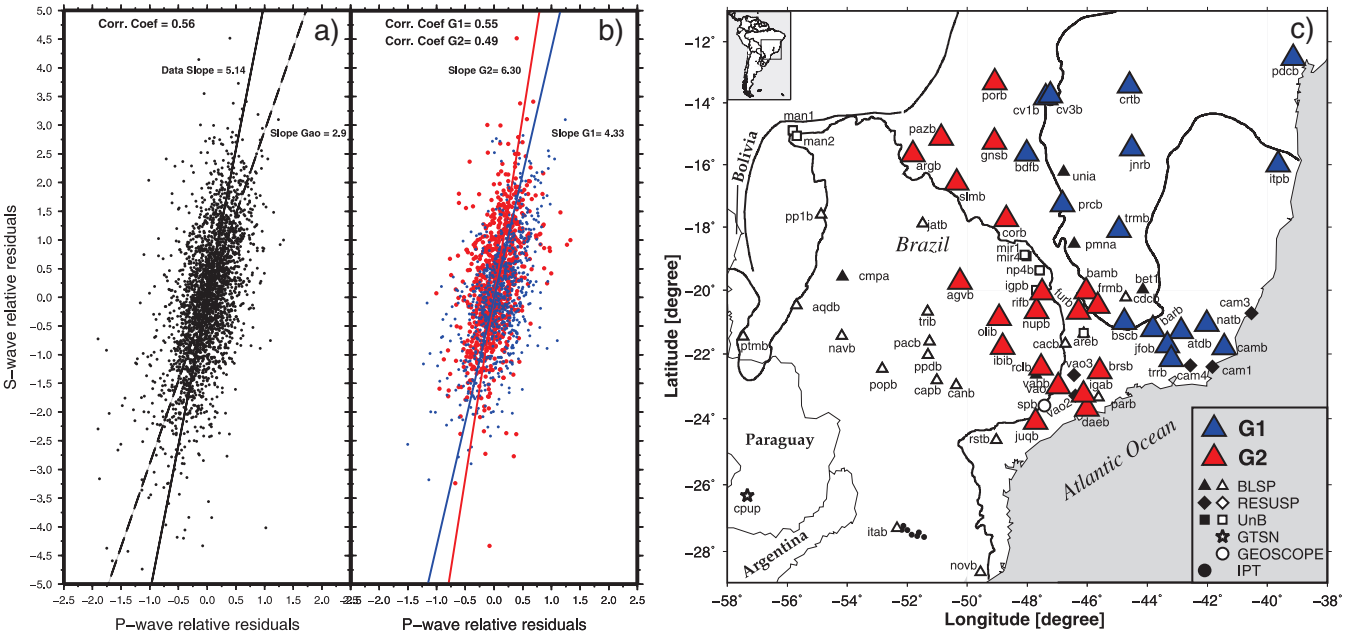

Figure 10. (a) *P*- versus *S*-wave relative traveltime residuals for common earthquakes and stations. The solid and dashed lines show the least-square fit and a slope of 2.9 for reference, respectively. (b) The red and blue dots show the *P*- versus *S*-wave traveltime residuals for the areas shown in (c). (c) The red and blue symbols mark the stations used for the measurements shown in (b).

least-square line through the measurements has a slope of 5.14. The total number of common *P*- and *S*-wave measurements is 2496 and the calculated correlation coefficient is 0.56 (significance is better than 95 per cent). Correlations with slope larger than 2.9 (Gao *et al.* 2004) cannot be explained by purely thermal anomalies (Karato 1993).

Fig. 10(b) shows *S*- versus *P*-wave relative traveltime residuals for stations deployed in two different areas (G1 and G2) which are shown in Fig. 10(c). It can be observed that the slope is slightly lower for the stable SFC (G1) than for the younger fold belts (G2). Still, the observed slopes are significantly larger than 2.9. We believe that the overall large slope is not due to shallow structures, which likely cause a higher variability through the different geological regimes. It therefore seems that deeper structures in the upper mantle and top of the lower mantle are responsible for these slopes. One possible explanation is that the large low velocity anomaly, which had been interpreted as the fossil conduct of the initial Tristan da Cunha Plume (VanDecar *et al.* 1995) has a chemical rather than thermal origin. The slopes are higher for stations deployed in the fold belts than in the cratonic area. This could be explained by the observed alkaline intrusions related to the Trindade plume track and the feeding of the Paraná flood basalts due to the starting Tristan da Cunha plume. All these geological signatures are visible at the Earth surface in the Paraná basin and fold belts, but not in the SFC.

Seismic anomalies in the tomographic images may also be related to artefacts of the inversion mainly due to the highly variable resolution (see Section 5) and due to the adopted approximations of the approach. In our study, we assume isotropic velocity anomalies. However, SK(K)S-splitting studies (Assumpção *et al.* 2006) in the area show fast polarization directions close to the absolute plate motions with signature of deflection by the root of the SFC. The teleseismic *P*-waves propagate perpendicular to the horizontal mantle flow direction and should therefore not affect our tomographic inversion results. The *S*-waves are more sensitive to anisotropy than *P*-waves but due to the good event coverage the effect of the azimuthal dependent anisotropy should be largely cancelled out in the inversion. Constant contributions of an anisotropic layer would be removed by the usage of relative residuals while random contributions are cancelled out. We cannot exclude artefacts due to anisotropy, but we believe that these artefacts are neglectable or weak and do not influence significantly our interpretations since the *P*- and *S*-wave models resemble each other despite their independent databases and different sensibility to anisotropy. Our tectonic interpretations in the *S*-wave model are therefore backed-up by the *P*-wave model.

The visual perception of seismic heterogeneities in our tomographic images may vary depending on the average velocity at each depth. We use relative traveltime residuals and loose therefore the ability to invert for the absolute velocities (e.g. see figure 13 in Schimmel *et al.* 2003). The blue and red colours mark thus only lateral velocity changes. In principal, a red anomaly can be a fast velocity anomaly with respect to the global average if the local average is faster since the study volume is located in an old shield. However, an overall abnormal velocity average, which may bias our images is not expected due to the large surface area of our study volume, which comprises different tectonic regimes of different ages (Proterozoic belts and Precambrian shields) without the dominance of one of these regimes. The map of one-way *S*-vertical traveltime residuals in Poupinet *et al.* (2003) confirms the presence of positive and negative traveltime residuals for our study area.

7 DISCUSSION

7.1 São Francisco Craton

Due to the installation of stations in the northern and western SFC, a high-velocity anomaly can be now observed in these portions of the SFC. The anomaly is more intense in the southern than in the northern part. Resolution tests show that the northern part has low resolution due to a poor data sampling in this region. The

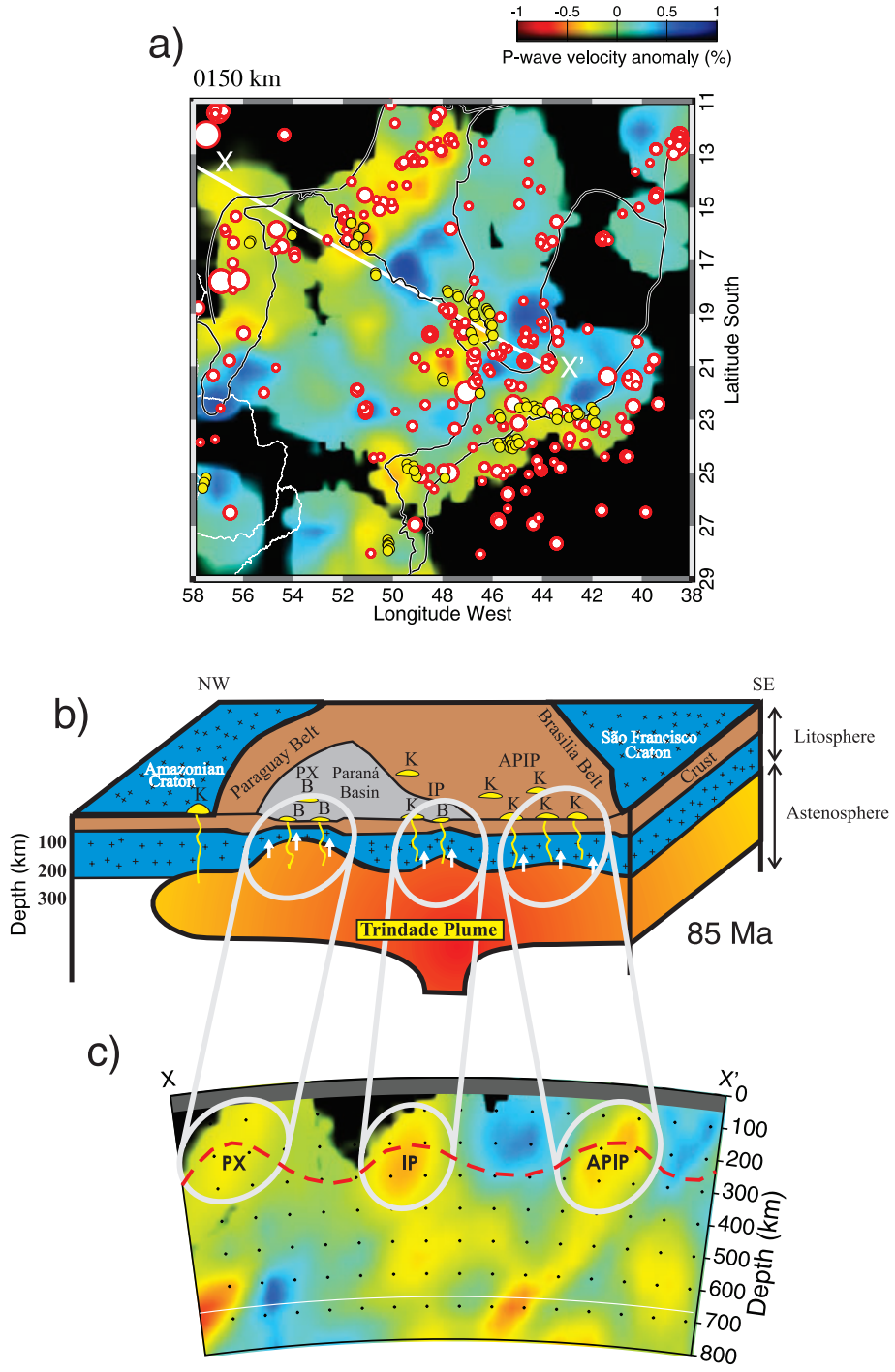

Figure 11. Comparison of the *P*-wave tomographic results with the model proposed by Gibson *et al.* (1995, 1997) to explain the presence of Upper Cretaceous alkaline intrusions. (a) Comparison between seismic tomography and the regional seismicity, mainly in the São Francisco Craton region. (b) Model proposed by Gibson *et al.* (1995, 1997), relating the origin of the Upper Cretaceous intrusions with the initial impact of the Trindade Plume. The hatched red line in (c) sketches the Lithosphere–Asthenosphere Boundary (LAB).

southern and western areas are better resolved owing to the higher station density. The high-velocity anomaly in the western limit of this craton (and beyond the surface geological limit) supports the hypothesis that this craton was part of a large Neoproterozoic plate (San Franciscan Plate-–Alkmin *et al.* 1993; Ussami 1993, 1999).

Fig. 11 shows the earthquake locations obtained from the IAG-USP hypocenter database between the years 1720 and 2004 on top of a horizontal cross-section for *P*-wave velocity anomalies at 150 km depth. According to Assumpção *et al.* (2004a) the seismicity in this area can be explained by stress concentration in the upper crust due to weaknesses in the lithosphere. As can be seen from Fig. 11, most of the events occur in the Tocantins Province, contouring the high-velocity anomaly obtained from seismic tomography. This indicates that it is the suture zone of the collision between the San Francisco Block and the Amazon and Paranapanema Blocks. Further, directions of the polarization of the fast split SKS waves

(Assumpção *et al.* 2006) show a fan shaped feature which opens to the east around this anomaly, suggesting an asthenospheric flow around the keel of this hypothetical San Franciscan Plate.

Vertical images for *P*- and *S*-wave velocity anomalies (Figs 7a and b), show the craton as a high velocity body until depths of 250 km. This depth is an overestimation due to vertical smearing and we believe, based in our synthetic tests, that a depth around 200 km is more appropriate for the root of the craton.

7.2 Low-velocity anomalies

At shallower depths (100–250 km), most low-velocity anomalies coincide with the provinces of alkaline intrusions of the Early Cretaceous (Fig. 11). The younger igneous provinces (85-50 MA), such as the Alto do Paranaíba (APIP), Iporá (IP) and Poxoréu (PX) Igneous Provinces are likely related with the Trindade Plume as proposed by Gibson *et al.* (1995) and Gibson *et al.* (1997) (Fig. 11).

According to Gibson *et al.* (1997), the initial impact of the Trindade Plume would have occurred below IP and would then have been dispersed to generate other igneous provinces through pockets of partial melt in thin lithospheric spots. The corresponding seismic anomalies, likely with a strong compositional component as can explain the slopes of Fig. 10, are observed in our tomographic images (Fig. 11) and are also confirmed by inversions of magnetotelluric data (Bologna *et al.* 2006).

According to Assumpção *et al.* (2004a) the intraplate seismicity in this area can be explained as a result of the concentration of stress in the upper crust due to a weak and thin lithosphere. Zones of the weakness could be caused by temperature anomalies on the order of 100°C or more (Assumpção *et al.* 2004a). It can be seen from Fig. 11 that there is a tendency of seismic activity in areas with low-velocity anomalies in the lithosphere.

The low-velocity anomaly interpreted by VanDecar *et al.* (1995) as being the fossil conduct of the initial Tristan da Cunha Plume (eastern part of the Paraná Basin) appears now better defined due to the data increase. Still, its base is not well imaged, but we believe that this anomaly does not extend much below 700 km based on synthetic tests. This low-velocity anomaly occupies a large volume below the centre of our study area and is therefore a likely source of the high slope obtained from the common *P*- and *S*-wave correlations shown in Fig. 10. Slopes higher than four are observed for the different regions in our study area. Compositional anomalies need to be invoked to explain slopes above 2.9 (Karato 1993). A common and deep source is the easiest explanation. In the regions of highest slope (fold belts, 6.3) the relation of low velocity anomalies and the presence of alkaline intrusions (kamafugites, lamproites and kimberlites) indicates that these anomalies have a compositional origin related to their melt sources. In fact, different heterogeneous mantle sources (e.g. due to different depth) have been proposed to explain variations in the composition of the alkaline intrusions (e.g. Gibson *et al.* 1995, Bologna *et al.* 2006).

7.3 Cratonic basement of the Paraná Basin

The high-velocity anomaly under the Paraná Basin is now better defined than in previous studies (VanDecar *et al.* 1995; Schimmel *et al.* 2003) due to the increased amount of data. Based on our results it is possible to test the model of several cratonic blocks, separated by suture zones according to Milani & Ramos (1998), as alternative to the unique cratonic nucleus proposed by Cordani *et al.* (1984) and Mantovani *et al.* (2005). Fig. 12 shows a comparison between these three models with a tomographic image at 150 km depth (Fig. 12c).

The model of Milani & Ramos (1998) seems to be better correlated with the tomographic anomalies. The low-velocity anomalies coincide well with the limits of the cratonic fragments proposed by Milani & Ramos (1998), mainly in the central region of the model, where there are more stations and the anomalies are better resolved. This indicates the presence of suture zones between these blocks. The southwest part of the high-velocity anomaly under the Paraná Basin is not well resolved, because of the poor station coverage in this region. Moreover, as shown in the synthetic tests this anomaly is influenced by the smearing of the anomaly attributed to the Nazca Plate. Receiver function analyses by Julià *et al.* (2008) showed that high velocities in the lower crust (indicative of possible underplating) tend to occur near the proposed suture zones of the model of Milani & Ramos (1998).

7.4 Nazca plate

The anomaly interpreted as the subducted Nazca Plate is orientated NW–SE (Figs 5 and 6) and follows the contour of the Andean Belt. The anomaly is oriented roughly parallel to the outline of the Nazca Plate as suggested by Cahill & Isacks (1992) based on the deep Andean seismicity (Fig. 13). However, due to the low station density and poor ray crossings, this structure appears stained upwards, where it interferes with shallower structures and where it inhibits a separation of anomalies.

The resolution tests show that the reconstruction of the slab is accompanied by low-velocity artefacts. Similar low-velocity structures appear in the real data reconstructions. We therefore believe that the low-velocity anomalies at larger depth besides the slab are artefacts due to our inversion. In fact, the appearance of these artefacts additionally strengthens the presence of the slab in the uppermost part of the lower mantle underneath Brazil. We do not refrain from the presentation of these noisier reconstructions at the top of the lower mantle since they still constrain real structures. Further, it shows the importance of resolution tests in the interpretation of tomographic images.

8 CONCLUSIONS

The new stations allowed to image high-velocity anomalies in the northern part of the SFC and allowed to observe that the craton is further extended to the west. This strengthens that the SFC was part of a larger San Franciscan Plate as proposed by Alkmim *et al.* (1993).

It seems that we start to resolve different high velocity anomalies in the lithosphere of the Paraná Basin. This would strengthen the proposed model by Milani & Ramos (1998) with several cratonic blocks separated by suture zones as opposed to a unique block proposed by Cordani *et al.* (1984) and Mantovani *et al.* (2005).

We observe in our results that the anomaly related to the Nazca Slab follows the outline of the Andean Belt. Due to the poor ray crossings in this area this structure appears smeared upwards, influencing other shallower structures.

At shallower depths, most low-velocity anomalies coincide with the provinces of Upper Cretaceous alkaline intrusions. The youngest igneous provinces (with ages between 85 and 50 MA) could be related to the Trindade Plume, as proposed by Gibson *et al.* (1995, 1997). There is a tendency of correlation between low velocity anomalies and areas with higher seismicity, which could

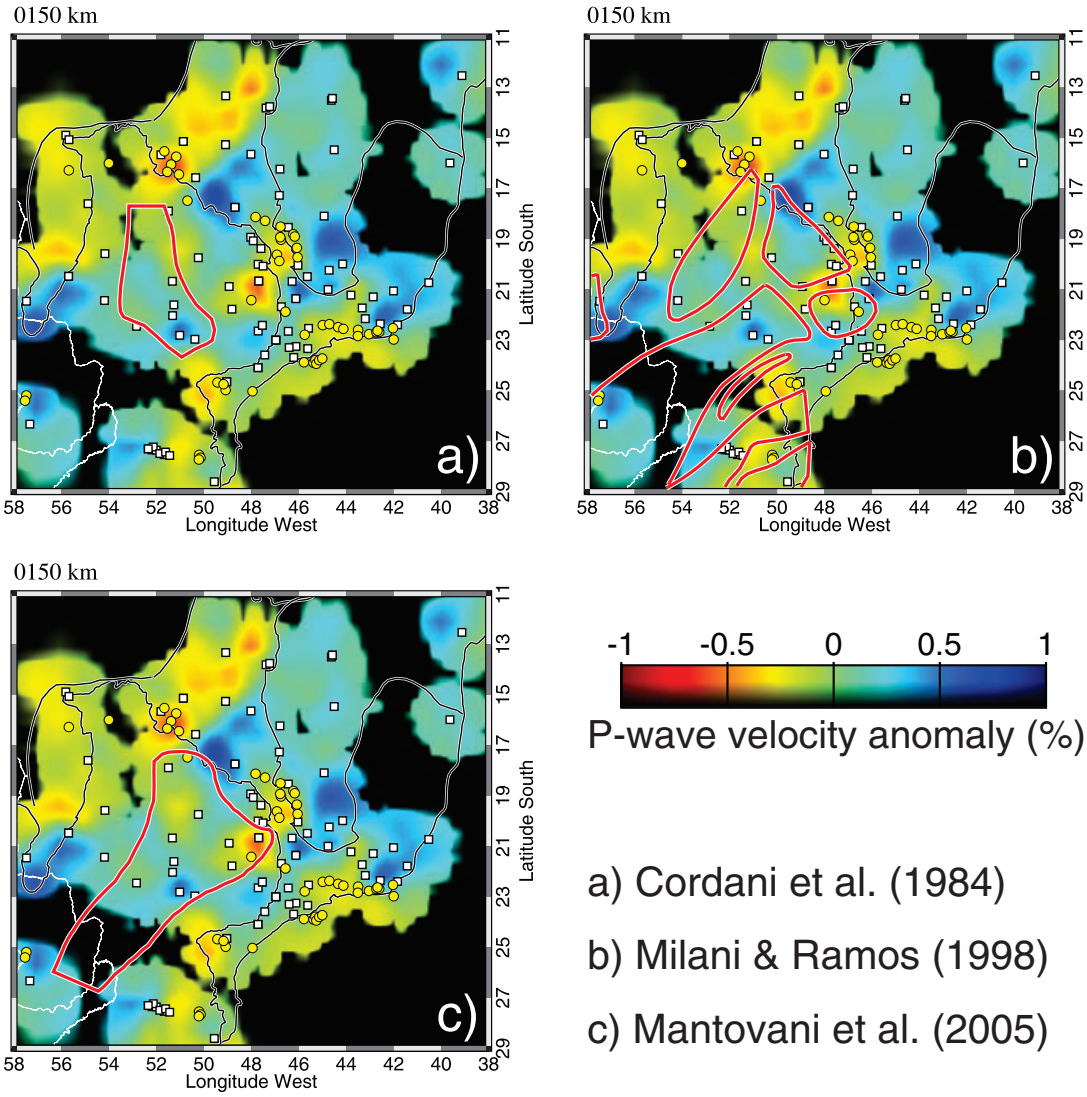

Figure 12. Comparison between the different models for the basement of the Paraná Basin with our *P*-velocity anomalies at 150 km depth.

indicate stress concentration in the upper crust caused by lithospheric thinning (possibly related to the impact of warm material from a Trindade Plume). The deep (300–700km) low-velocity anomaly interpreted by VanDecar *et al.* (1995) was better resolved in our results.

The test inversions of synthetic data proved to be essential in our analysis, since the resolution varies throughout our study volume. It could be shown that the low velocity anomalies besides the Nazca Plate are artefacts due to the data and inversion approach. Their appearance in the real images strengthens the presence of the Nazca Plate.

Comparison between *P*- and *S*-wave relative residual suggests that the influence of temperature and composition in the seismic anomalies are different in distinct regions. The slope of the *P*- versus *S*-wave relative traveltime correlations is slightly larger for measurements from areas with mainly low-velocity anomalies than for measurements taken from the stable craton. This might be due to the presence of alkaline intrusions caused by the earlier occurrence of partial melting in the region. In any case, compositional heterogeneities are expected to explain the slopes in both areas. A possible explanation of this observation is that the large low-velocity anomaly in the centre of our study volume, previously interpreted as related to the Tristan da Cunha Plume, is actually a compositional anomaly.

ACKNOWLEDGMENTS

Work supported by Brazilian grants FAPESP 05/51035-2, 01/06066-6 and CNPq 30.4809/2003-9, 141318/2004-0, 20.3726/2005-7. We are grateful to Institute of Technological Research of São Paulo, Seismological Observatory of the University of Brasilia, GTSN and GEOSCOPE Networks and also Suzan Van der Lee (ETH-Z) for sharing part of the data used in this work. The Regional Seismic Tomography code was kindly provided by John VanDecar. We thank José Roberto Barbosa for help during field work and also Luís Galhardo and Dennis Schramm for equipment service and maintenance during the tomography experiment. The constructive reviews by the associate editor Gabi Laske, the referee Uli Achauer and an anonymous referee improved the manuscript. MS acknowledges PN No. CGL2006-01171 (S-Iberia). Maps were

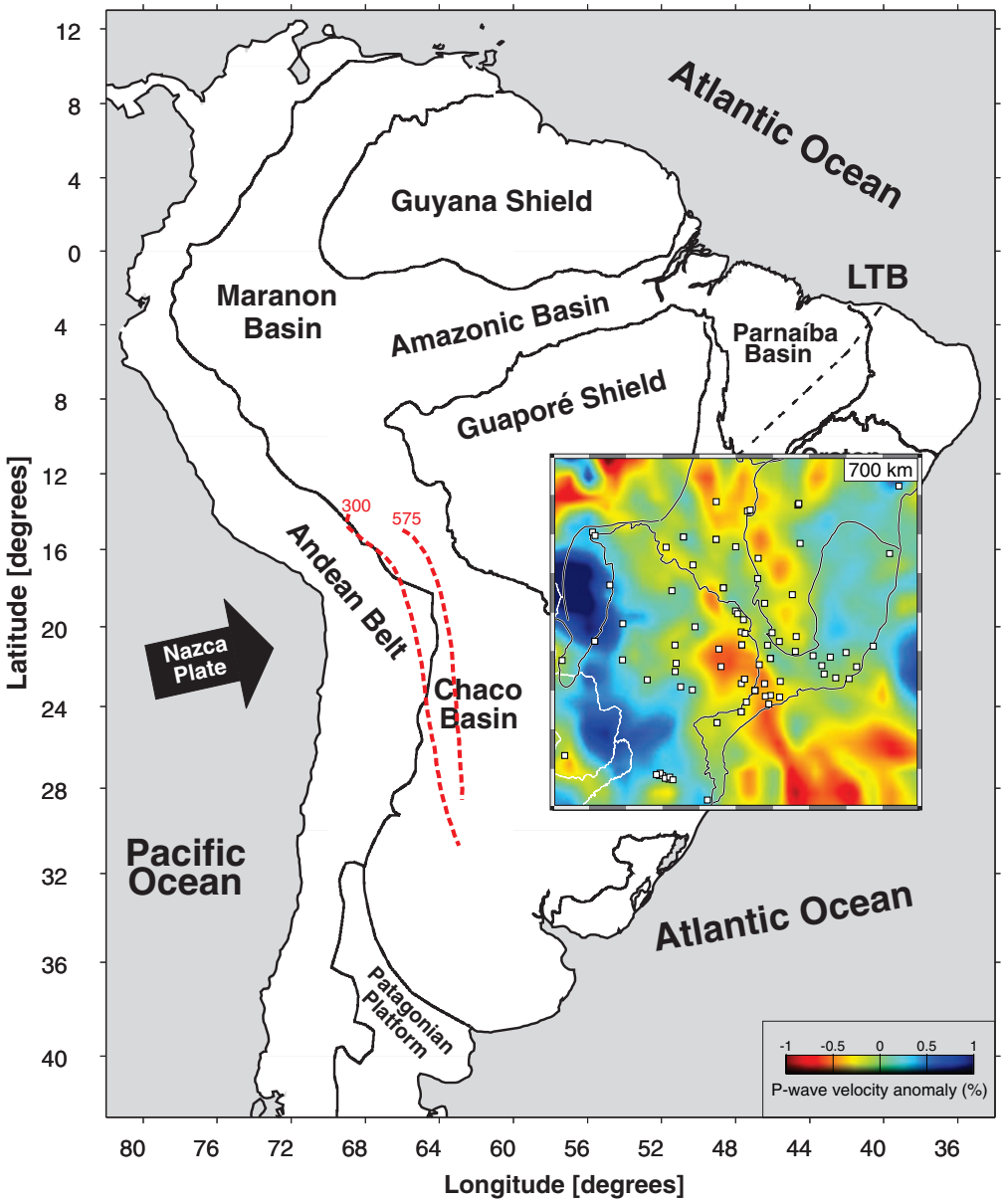

Figure 13. Seismic anomalies at 700 km depth. This anomaly is consistent with the outline of the Nazca Plate suggested by Cahill & Isacks (1992) based on the Andean Seismicity.

plotted using GMT (Wessel & Smith 1991) and seismograms were analysed with SAC (Goldstein *et al.* 2003).

REFERENCES

Alkmim, F.F., Brito Neves, B.B. & Barbosa, J.S.F., 1993. Arcabouço tectônico do Cráton do São Francisco – uma revisão, in *O Cráton do São Francisco,* pp. 45–62, eds Dominguez, J.M.L. & Misi, A., SBG Núcleo Bahia/Sergipe, Salvador.

Alkmim, F.F. & Cruz, S.C.P., 2005. Cratógenos, aulacogenos, orógenos e suas interações: O caso do Cráton do São Francisco-Congo e sistemas brasilianos/pan-africanos adjacentes, *III Simpósio sobre o Cráton do São Francisco*, 185–187.

Almeida, F.F.M., Brito Neves, B.B. & Dal Re Carneiro, C., 2000. The origin and evolution of the South American platform, *Earth-Sci. Rev.,* **50**(1–2), 77–111, doi:10.1016/S0012-8252(99)00072-0.

Artemieva, I.M., Billien, M., Lévêque, J. & Mooney, W.D., 2004. Shear wave velocity, seismic attenuation, and thermal structures of the continental upper mantle, *Geophys. J. Int.,* **157,** 607–628, doi:10.1111/j.1365-246X.2004.02195.x.

Assumpção, M., An, M., Bianchi, M., França, G.S.L., Rocha, M., Barbosa, J.R. & Berrocal, J., 2004a. Seismic studies of the Brasilia fold belt at the western border of the São Francisco Cráton, Central Brazil, using receiver function, surface-wave dispersion and teleseismic tomography, *Tectonophysics,* **388,** 173–185, doi:10.1016/j.tecto.2004.04.029.

Assumpção, M., Schimmel, M., Escalante, C., Rocha, M. Barbosa, J.R. & Barros, L.V., 2004b. Intraplate seismicity in SE Brazil: stress concentration in lithospheric thin spots, *Geophys. J. Int,* **159,** 390–399, doi:10.1111/j.1365-246X.2004.02357.x.

Assumpção, M., Heintz, M., Vauchez, A. & Silva, M., 2006. Upper mantle anisotropy in SE and Central Brazil from SKS splitting: Evidence of asthenospheric flow around a cratonic keel, *Earth planet. Sci. Lett.,* **250,** 224–240, doi:10.1016/j.epsl.2006.07.038.

Bastow, I.D., Stuart, G.W., Kendall, J.M. & Ebinger, C.J., 2005. Upper-mantle seismic structure in a region of incipient continental breakup: Northern Ethiopian rift, *Geophys. J. Int.,* **162**(2), 479–493, doi:10.1111/j.1365-246X.2005.02666.x.

Bastow, I.D., Nyblade, A.A., Stuart, G.W., Rooney, T.O. & Benoit, M.H., 2008. Upper mantle seismic structure beneath the Ethiopian hotspot: Rifting at the edge of the African low velocity anomaly, *Geochem. Geophys. Geosyst.,* **9**(Q12022), 25 pp., doi:10.1029/2008GC002107.

Benoit, M.H., Nyblade, A.A. & VanDecar, J.C., 2006. Upper mantle P-wave speed variations beneath Ethiopia and the origin of the Afar hotspot, *Geology,* **34**(5), 329–332, doi:10.1130/G22281.1.

Bologna, M.S., Padilha, A.L., Vitorello, I. & Fontes, S.L., 2006. Tectonic insight into a pericratonic subcrustal lithosphere affected by anorogenic Cretaceous magmatism in central Brazil inferred from long-period magnetotellurics, *Earth planet. Sci. Lett.*, **241**(3–4), 603–616, doi:10.1016/j.epsl.2005.11.022.

Brito Neves, B.B. & Cordani, U.G., 1991. Tectonic evolution of South America during the Late Proterozoic, *Precambrian Res.,* **53**, 23–40, doi:10.1016/0301-9268(91)90004-T.

Cahill, T. & Isacks, B., 1992. Seismicity and shape of the subducted Nazca Plate, *J. geophys.Res.,* **97**(B12), 17503–17529, doi:10.1029/92JB00493.

Cline, A.K., 1981. *FITPACK – Software package for curve and surface fitting employing splines under tension,* Department of Computer Sciences, University of Texas, Austin.

Constable, S.C., Parker, R.L. & Constable, C.G., 1987. Occam's inversion: a pratical algorithm for generation smooth models from electromagnetic sounding data, *Geophysics,* **52,** 289–300, doi:10.1190/1.1442303.

Cordani, U.G. & Sato, K., 1999. Crustal evolution of the South American Platform, based on Nd isotopic systematics on granitoids rocks, *Episodes,* **22**(3), 167–173.

Cordani, U.G., Fuck, R.A., Brito Neves, B.B., Filho, A.T. & Cunha, F.M.B., 1984. Estudo preliminar de integração do Pré-Cambriano com os eventos tectônicos das Bacias Sedimentares Brasileiras, Revista Ciência-Técnica-Petróleo, Seção Exploração de Petróleo, Petrobras/Cenpes/Sintep, Publicação no.: 15.

Cordani, U.G., Sato, K., Teixeira, W., Tassinari C.C.G. & Basei, M.A.S., 2000. Crustal evolution of the South American platform, in *Tectonic Evolution of South America,* pp. 19–40, eds Cordani, U.G., Milani, E.J., Thomaz-Filho, A. & Campos, D.A., Finep, Brazil.

Deschamps, F., Trampert, J., & Snieder, R., 2002. Anomalies of temperature and iron in the uppermost mantle inferred from gravity data and tomographic models, *Phys. Earth planet. Inter.,* **129**, 245–264, doi:10.1016/S0031-9201(01)00294-1.

Escalante, C., 2002. Tomografia sísmica do manto superior sob o sudeste e centro oeste do Brasil, *M. Phil thesis*. IAG/USP, São Paulo, SP, p. 74.

Evans, J.R. & Achauer, U., 1993. Teleseismic velocity tomography using the ACH-method: theory and application to continental scale studies, in *Seismic Tomography: Theory and Practice,* pp. 319–360, ch. 13, eds Iyer, H.M. & Hirahara, K., Chapman and Hall, London.

Feng, M., Assumpção, M.S. & Van Der Lee, S., 2004. Group-velocity tomography and lithospheric S-velocity structure of the South American continent, *Phys. Earth planet. Inter.,* **147,** 315–331, doi:10.1016/j.pepi.2004.07.008.

Feng, M., Van Der Lee, S. & Assumpção, M., 2007. Upper mantle structure of South America from joint inversion of waveforms and fundamental mode group velocities of Rayleigh waves, *J. geophys. Res.*, **112**(B04312), 16 pp, doi:10.1029/2006JB004449.

Fyfe, W.S. & Leonardos Jr. O.H., 1974. Ancient metamorphic-migmatite belts of the Brazilian Atlantic coast: the African conection, *Rev. Brasileira de Geociências,* **4,** 247–252.

Gao, W., Grand, S.P., Baldridge, W.S., Wilson, D., West, M., Ni, J.F. & Aster, R., 2004. Upper mantle convection beneath the central Rio Grande rift imaged by P- and S wave tomography, *J. geophys. Res.,* **109**(B03305), doi:10.1029/2003JB002743.

Gibson, S.A., Thompson, R.N., Leonardos, O.H., Dickin, A.P. & Mitchell, J.G., 1995. The late Cretaceous impact of the Trindade mantle plume: evidence from large-volume, mafic, potassic magmatism in SE Brazil, *J. Petrol.,* **36**(1), 189–229, doi:10.1093/petrology/36.1.189.

Gibson, S.A., Thompson, R.N., Weska, A.P., Dickin, A.P. & Leonards, O.H, 1997. Late Cretaceous rift-related upwellings and melting of the Trindade starting mantle plume head beneath western Brazil, *Contrib. Mineral. Petrol.,* **126,** 303–314, doi:10.1007/s004100050252.

Gibson, S.A., Thompson, R.N., Day, J.A., Humphris, S.E. & Dickin, A.P., 2005. Melt-generation processes associated with the Tristan mantle plume: constraints on the origin of EM-1, *Earth planet. Sci. Lett.,* **237**(3–4), 744–767, doi:10.1016/j.epsl.2005.06.015.

Goes, S., Govers, R. & Vacher, P., 2000, Shallow mantle temperatures under Europe from P and S wave tomography, *J. geophys. Res.,* **105**(B5), 11 153–11 169, doi:10.1029/1999JB900300.

Goldstein, P., Dodge, D., Firpo, M. & Lee Minner, 2003. 85.5 SAC2000: Signal processing and analysis tools for seismologists and engineers, in *International Geophysics, Part 2, International Handbook of Earthquake and Engineering Seismology*, Vol. 81, pp. 1613–1614, eds Lee, W.H.K., Kanamori, H., Jennings, P.C. & Kisslinger, C., Academic Press, London, doi:10.1016/S0074-6142(03)80284-X.

Heilbron, M., Pedrosa-Soares, A., Neto, M., da Silva, L., Trouw, R. & Janasi, V., 2004. Brasiliano Orogens in Southeast and South Brazil, *J. Virtual Explorer*, **17,** paper 4.

Heintz, M., Debayle, E. & Vauchez, A., 2005. Upper mantle structure of the South American continent and neighboring oceans from surface wave tomography, *Tectonophysics,* **406,** 115–139, doi:10.1016/j.tecto.2005.05.006.

Huber, P.J., 1981. *Robustic Statistics,* Wiley, New York.

Julià, J., Assumpção, M. & Rocha, M.P., 2008. Deep crustal structure of the Paraná Basin from receiver functions and Rayleigh-wave dispersion: evidence for a fragmented cratonic root, *J. geophys. Res.,* **113,** B08318, doi:10.1029/2007JB005374.

Karato, S., 1993. Importance of anelasticity in the interpretation of seismic tomography, *Geophys. Res. Lett.,* **20**(15), 1623–1626, doi:10.1029/93GL01767.

Karato, S. & Karki, B.B., 2001. Origin of lateral variation of seismic wave velocities and density in the deep mantle, *J. geophys. Res.,* **106**(B10), 21 771–21 783, doi:10.1029/2001JB000214.

Kennett, B.L.N. & Engdahl, E.R., 1991. Travel-times for global earthquakes location and phase identification, *Geophys. J. Int.,* **105,** 429–465, doi:10.1111/j.1365-246X.1991.tb06724.x.

Lees, J.M., VanDecar, J., Gordeev, E., Ozerov, A., Brandon, M., Park, J. & Levin, V., 2007. Three dimensional images of the Kamchatka-Pacific Plate Cusp., in *Volcanism and Subduction: the Kamchatka region,* Geophys. Monogr. Ser. 172, pp. 65–75, eds Eichelberger, J., Gordeev, E., Kasahara, M., Tzbekov, P. & Lees, J., Am. geophys. Un., Washington, D.C.

Liu, K.H., Gao, S., Silver, P.G. & Zhang, Y., 2003. Mantle layering across central South América, *J. geophys. Res.,* **108**(B11), 2510, doi:10.10219/2002JB002208.

Mantovani, M.S.M., Quintas, M.C.L., Shukowsky, W. & de Brito Neves, B.B., 2005. Delimitation of the Paranapanema Proterozoic block: a geophysical contribution, *Episodes,* **28**(1), 18–22.

Milani, E.J. & Ramos, V.A., 1998. Orogenias paleozóicas no domínio sul-ocidental do Gondwana e os ciclos de subsidência da Bacia do Paraná, *Rev. Brasileira de Geociências,* **28**(4), 473–484.

Montes-Lauar, C.R., Pacca, I.G., Melfi, A.J. & Kawashita, K., 1995. Late Cretaceous alkaline complexes, southeastern Brazil: paleomagnetism and geochronology, *Earth planet. Sci. Lett.,* **134**(3–4), 425–440, doi:10.1016/0012-821X(95)00135-Y.

Neele, F., Vandecar, J. & Snieder, R., 1993. The use of P-wave amplitude data in a joint inversion with travel times for upper mantle velocity structure, *J. geophys. Res.,* **98,** 12033–12054.

Paige, C.C. & Saunders, M.A., 1982a. Algorithm 583, LSQR: sparse linear equations and least squares problems, *ACM Trans. Math. Softw.,* **8**(2), 195–209.

Paige, C.C. & Saunders, M.A., 1982b. LSQR: an algorithm for sparse linear equations and sparse least squares, *ACM Trans. Math. Softw.,* **8**(2), 43–71.

Pérez-Gussinyé, M., Lowry, A.R. & Watts, A.B., 2007. Efective elastic thickness of South America and its implications for intracontinental deformation, Geochem. *Geophys. Geosyst.,* **8**(5), 22, Q05009, doi:10.1029/2006GC001511.

Pimentel, M.M., Fuck, R.A., Jost, H., Filho, C.F.F. & Araújo, S.M., 2000. The basement of the Brasília Fold Belt and the Goiás, in *Tectonic Evolution of South America Magmatic Arc, 195-229,* 31st International Geological Congress, Rio de Janeiro, Brazil.

Poupinet, G., Arndt, N. & Vacher, P., 2003. Seismic tomography beneath stable tectonic regions and the origin and composition of the continental lithospheric mantle, *Earth planet. Sci. Lett.,* **212**(1–2), 89–101, doi:10.1016/S0012-821X(03)00258-9.

Pulliam, R.J., Vasco, D.W. & Johnson, L.R., 1993. Tomographic inversions for mantle P wave velocity structure based on the minimization of l2 and l1 norms of international seismological centre travel-time residuals, *J. geophys. Res.,* **98**(B1), 699–734, doi:10.1029/92JB01053.

Ramos, V., 1999. Plate tectonic setting of the Andean Cordillera, *Episodes,* **22**(3), 183–190.

Rawlinson, N., Reading, A.M. & Kennett, B.L.N., 2006. Lithospheric structure of Tasmania from a novel form of teleseismic tomography, *J. geophys. Res.,* **111**(B02301), 21 pp, doi:10.1029/2005JB003803.

Ren, Y., Stutzmann, E., Van Der Hilst, R.D. & Besse, J., 2007. Understanding seismic heterogeneities in the lower mantle beneath the Americas from seismic tomography and plate tectonic history, *J. geophys. Res.,* **112**(B01302), doi:10.1029/2005JB004154.

Rocha, M.P., 2003. Ampliação da Tomografia Sísmica do Manto Superior no Sudeste e Centro-Oeste do Brasil com ondas P, *M.Phil thesis* – IAG-USP, São Paulo, p. 71.

Schmid, C., Van Der Lee, S., VanDecar, J.C., Engdahl, E.R. & Giardini, D., 2008. Three-dimensional S velocity of the Mantle in the Africa-Eurasia Plate boundary region from phase arrival times and regional waveforms, *J. geophys. Res.,* **113**(B03306), doi:10.1029/2005JB004193.

Schimmel, M., 1999. Phase Cross-Correlation: Design, Comparison, and Application, *Bull. seism. Soc. Am.,* **89,** 1366–1378.

Schimmel, M., Assumpção, M. & VanDecar, J.C., 2003. Seismic velocity anomalies beneath SE Brazil from P- and S wave travel-time inversions, *J. geophys. Res.,* **108**(1–13), doi:10.1029/2001JB000187.

Siebel, W., Becchio, R., Volker, F., Hansen, M.A.F., Viramonte, J., Trumbull, R.B., Haase, G. & Zimmer, M., 2000. Trindade and Martin Vaz Islands, South Atlantic: Isotopic (Sr, Nd, Pb) and trace element constraints on plume related magmatism, *J. South Am. Earth Sci.,* **13**(1–2), 79–103, doi:10.1016/S0895-9811(00)00015-8.

Silva, L.C., McNaughton, N.J., Armstrong, R., Hartmann, L.A. & Fletcher, I.R., 2005. The neoproterozoic Mantiqueira Province and its African connections: a zircon-based U-Pb geochronologic subdivision for the Brasiliano/Pan-African systems of orogens, *Precambrian Res.,* **136**(3–4), 03–240, doi:10.1016/j.precamres.2004.10.004.

Sol, S., Thomsom, C.J., Kendall, J-M., White, D., VanDecar, J.C. & Asudeh, I., 2002, Seismic tomographic images of the cratonic upper mantle beneath the Western Superior Province of the Canadian Shield – A remnant Archean slab?, *Phys. Earth planet. Inter.,* **34,** 53–69, doi:10.1016/S0031-9201(02)00081-X.

Teixeira, W., Sabaté, P., Barbosa, J., Noce, C.M. & Carneiro, M.A., 2000. Archean and Paleoproterozoic tectonic evolution of the São Francisco Craton, Brazil, in *Tectonic Evolution of South America,* pp. 101–137, eds Cordani, U.G., Milani, E.J., Thomaz-Filho, A. & Campos, D.A., Finep, Brazil.

Thompson, R.N., Gibson, S.A., Mitchell, J.G., Dickin, A.P., Leonards, O.H., Broad, J.A. & Greenwood, J.C., 1998. Migrating Cretaceous-Eocene Magmatism in the Serra do Mar Alkaline Province, SE Brazil: melts from deflected Trindade Mantle Plume? *J. Petrol.,* **39,** 1493–1526.

Ussami, N., 1993. Estudos Geofísicos no Cráton do São Francisco: Estágio Atual e Perspectivas, in *O Cráton do São Francisco,* pp. 35–43, eds Domingues, J. & Misi, A., Soc. Brasileira de Geologia, Brazil.

Ussami, N., 1999. Estruturação e Limites da Placa Litosférica São Franciscana: Contribuição Gravimétrica, Tese de livre docência, Universidade de São Paulo, 61.

VanDecar, J.C., James, D.E. & Assumpção, M., 1995. Seismic evidence for a fossil plume beneath South America and implications for plate driving forces, *Nature,* **378,** 25–31, doi:10.1038/378025a0.

VanDecar, J.C. & Crosson, R.S., 1990. Determination of telesseismic relative phase arrival times using multi-channel cross-correlation and least squares, *Bull. seism. Soc. Am.,* **80,** 150–169.

Van Der Lee, S. & Wiens, D.A., 2006. Seismological contraints on earth deep water cycle, in *Earth's Deep Water Cicle,* pp. 13–28, Vol. 168, eds Jacobsen, Steven D. & Suzan van, der Lee, Geophysical monograph series, AGU, Washington, D.C.

Wessel, P. & Smith, W.H.F., 1991. Free software helps map and display data, *EOS, Trans. Am. geophys. Un.,* **72**(41), p. 441, doi:10.1029/90EO00319.

West, J., Fouch, M., Roth, J. & Elkins-Tanton, L., 2009. Vertical mantle flow associated with a lithospheric drip beneath the Great Basin, *Nat. Geosci.,* **2**(6), 439–444, doi:10.1038/ngeo526.

Wolfe, C.J., Bjarnason, I.Th., VanDecar, J.C. & Solomon, S.C., 2002. Assessing the depth resolution of tomographic models of upper mantle structure beneath Iceland, *Geophys. Res. Lett.,* **29**(2), 1015, doi:10.1029/2001GL013657.

Zalán, P.V. *et al*. 1990. The Paraná Basin, Brazil, in *Interior Cratonic Basins*, Vol. 51, pp. 681–708, eds Leighton, M.W., Kolata, D.R., Oltz, D.F., Eidel, J.J., American Association of Petroleum Geologists Memoir, Tulsa.